3. INTERMEDIATE FIELD TEST 1

This section presents information on INEL ISV Intermediate Field Test 1 and includes the specific objectives of the test, construction of the test pit, and description and assessment of the data collected during process operations. Product durability data are presented in Section 5. Results of the test tracer study are presented in Section 6. And information from analytical modeling based on off-gassing is presented in Section 7.

3.1 Test 1 Objectives and Test Pit Overview

This section presents objectives and design considerations specific to Test 1. General objectives applicable to both ISV tests are presented in Section 2.1 (see p. 21).

Test Pit 1 was primarily designed to test the ISV process in an area of randomly disposed waste that was representative of conditions expected to exist at the SDA. Due to the nonhomogeneous character of the SDA waste and the uncertainties regarding characterization of the waste, it was possible to represent SDA waste only in an overall sense. However, several key aspects of SDA buried waste were represented in order to collect applicable data for ISV processing performance, namely, buried combustible material and buried scrap metal in containers. Because all the waste was contained in cans and boxes, significant void space in containers existed due to constraints on packing scrap materials. Containers with void spaces are typical of what may be expected within SDA buried waste.

3.2 Test Pit 1 Construction Details

From bottom to top, Test Pit 1 consisted of 0.6 m (2 ft) of soil underburden, 1.8 m (6 ft) of a randomly-disposed box and can layer mixed with fill dirt, and 0.6 m (2 ft) of soil overburden. Figure 10 is a schematic of the completed Test Pit 1 with the hood in place.

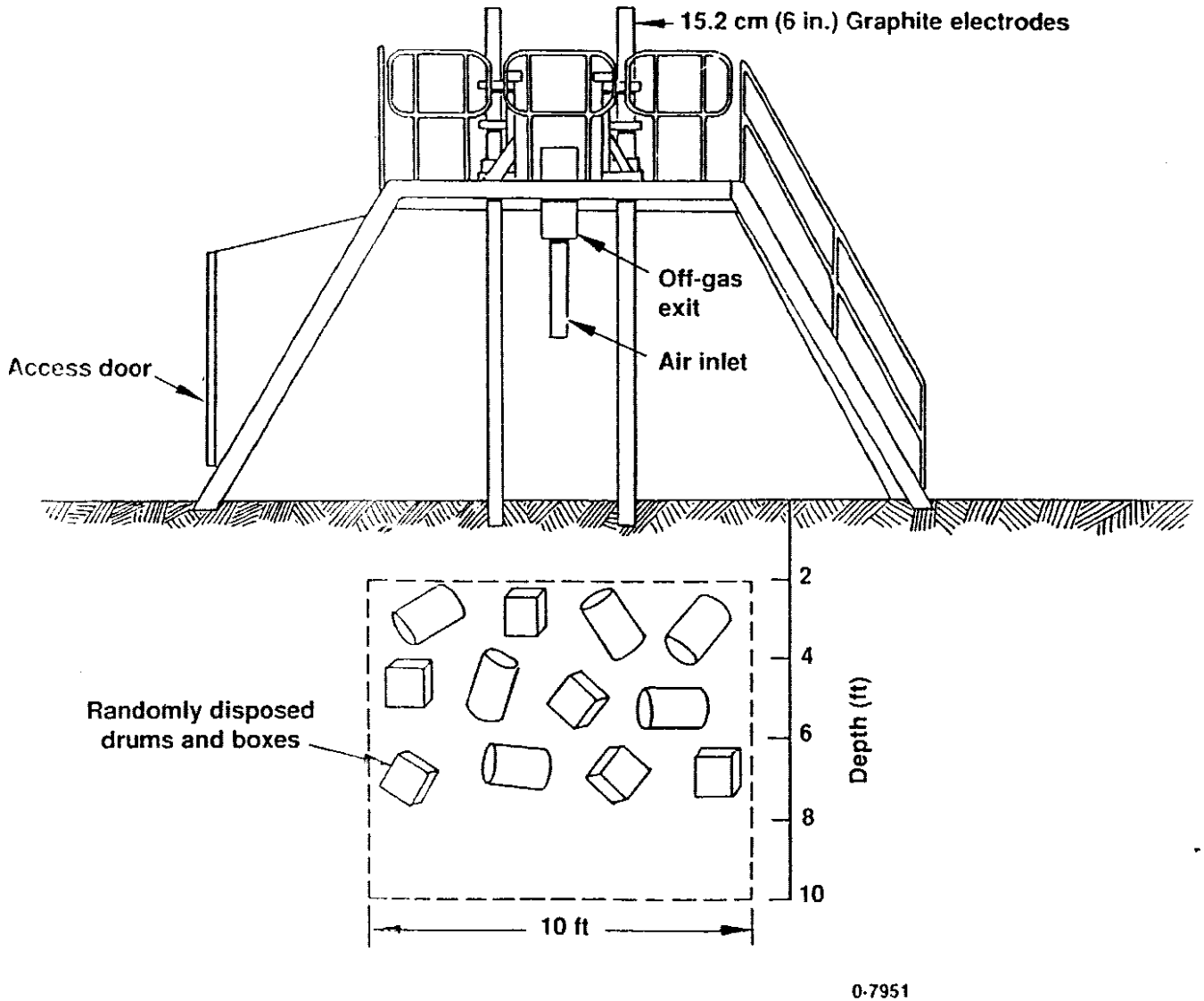

Figure 10. Schematic of completed Test Pit 1 with hood assembly covering the test site.

Test Pit 1 was built up in four layers with each layer consisting of approximately 5 boxes and 50 cans. The number of cans and boxes for each waste type in each layer is shown in Table 5. Tables 6 and 7 show the overall amounts of each waste type in the test pit. To obtain a random mixture of different waste types, a lottery was used to specify how many cans and boxes of each waste type would go into the specific layer being built. The cans and boxes were randomly placed into the test pit by hand with the exception of the cans containing tracers, which were hand-placed at specified levels and near the center of the pit.

Three types of tracer were place in Test Pit 1 in order to obtain data on possible effects of depth on tracer migration or release behavior. During Test Pit 1 filling, the three tracers were placed in three separate layers. Each tracer was added to six separate waste cans. The amount of tracer added to each can was approximately 225 g. The waste cans containing tracers were marked with orange spray paint and placed near the center of the pit to ensure that all tracer material would be within the melt zone. Figure 11 shows layer 4 (bottom layer of the four waste layers) after 5 boxes and 50 cans had been place. The boxes still banded to the wooden pallets contained concrete and glass; the other boxes contained scrap metal. Figure 12 shows layer 4 after backfill dirt has been added. Before starting on the next layer a hand compactor was used to compact the dirt. After compaction, layer 3 (second layer from the bottom of the pit) was placed containing 56 cans and 5 boxes. Figure 13 shows the cans and boxes for layer 2 (third layer from the bottom of the pit), which contained two tiers of tracer cans. The bottom tier of layer 2 contained tracer cans with ytterbium oxide, which were placed near the center of the pit. After placing backfill dirt over the bottom tier, the top tier was place with tracer cans containing terbium oxide, as shown in Figure 14. Figure 15 shows the can placement for layer 1 (the top layer), except for the tracer cans that contained dysprosium oxide.

During construction of Test Pit 1, two arrays of type K thermocouples were placed. A vertical array was place starting at approximately 15.2 cm (6 in.) from ground level and with the thermocouples spaced every 15.2 cm

Table 5. Depth view of Test Pit 1[a]

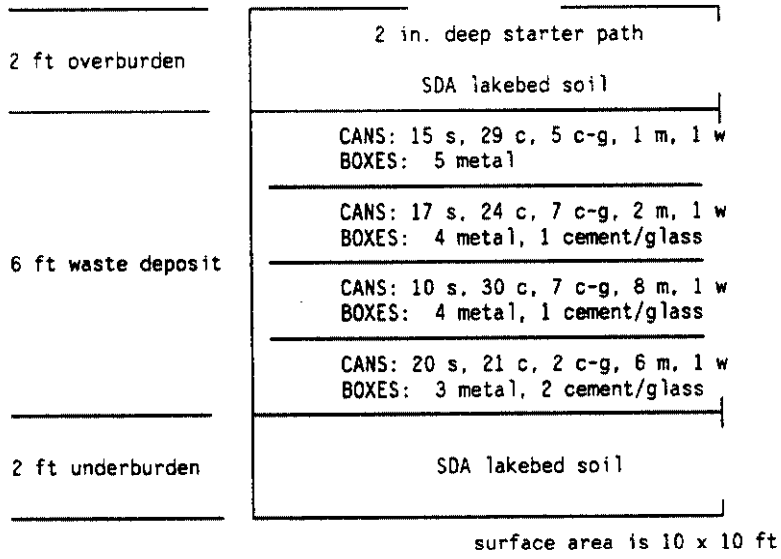

Where,

s is sludge cans

c is combustible cans

c-g is concrete/glass cans

m is metal cans

w is wood cans.

These designations indicate the contents of the cans. These cans contained the following, approximate amounts of material:

Sludge can (s) - 10.716 lb

(7.71 - H_2O, 0.70 - FLOOR DRI, 2.307 - MICRO-CEL E)

Combustible can (c) - 4.154 lb (1.637 - Cloth, 2.517 - Paper)

Concrete/glass can (c-g) - 17.440 lb (11.035 - concrete, 6.405 - glass)

Metal can (m) - 8.235 lb (4.118 - carbon steel, 4.118 stainless steel)

Wood can (w) - 4.875 lb

Pallet - 13.5 lb of wood

Boxes contained the following, approximate amounts of material:

Metal - 123.0625 lb (50% carbon steel)

Concrete/glass - 246.375 lb (158.75 - concrete, 87.625 - glass)

a. Engineering Design File, EDF-ISV-034.

Table 6. Test Pit 1 waste deposit material composition in pounds[a]

MATERIALS	TOTAL		ITEM WEIGHT	WASTE DEPOSIT LAYERS TOP	2ND	3RD	BOTTOM
COMBUSTIBLES:	665.5						
Cans:		451.5					
Paper			261.75	72.99	60.40	75.51	52.85
Cloth			170.25	47.47	39.29	49.11	34.38
Wood			19.50	4.88	4.87	4.88	4.87
Boxes:		214.0					
Cardboard			160.00	40.00	40.00	40.00	40.00
Pallet (wood)			54.00	0.00	13.50	13.50	27.00
SLUDGE: (cans only)	664.4						
Water		478.0	478.00	115.65	131.06	77.10	154.19
Floor Dri		43.4	43.40	10.50	11.90	7.00	14.00
Micro-Cel		143.0	143.00	34.50	39.20	23.10	46.20
METALS:	2,473.0						
Cans:		504.0					
Stainless			70.00	4.12	8.24	32.94	24.70
Carbon Steel			434.00	93.37	97.49	130.94	112.20
Boxes:		1,969.0					
Stainless			984.50	307.65	246.13	246.13	184.59
Carbon Steel			984.50	307.65	246.13	246.13	184.59
CONCRETE/GLASS:	1,351.75						
Cans:		366.25					
Concrete			231.75	55.18	77.25	77.25	22.07
Glass			134.50	32.03	44.83	44.83	12.81
Boxes:		985.5					
Concrete			635.00	0.00	158.75	158.75	317.50
Glass			350.50	0.00	87.62	87.63	175.25
TOTALS OF COLUMNS	5,154.65		5,154.65	1,125.99	1,306.66	1,314.80	1,407.20

a. Engineering Design File, EDF-ISV-034.

Table 7. Test Pit 1 waste inventory

Material	Mass (lb)	% of Total Mass
Combustible	666	1.1
Sludge		
Water	478	0.8
FLOOR-DRI	43	0.07
MICRO-CELL E	143	0.2
Metal	2473	4.1
Glass	485	0.8
Concrete	867	1.5
Soil (excluding underburden)	54,630	
Total	59,785	

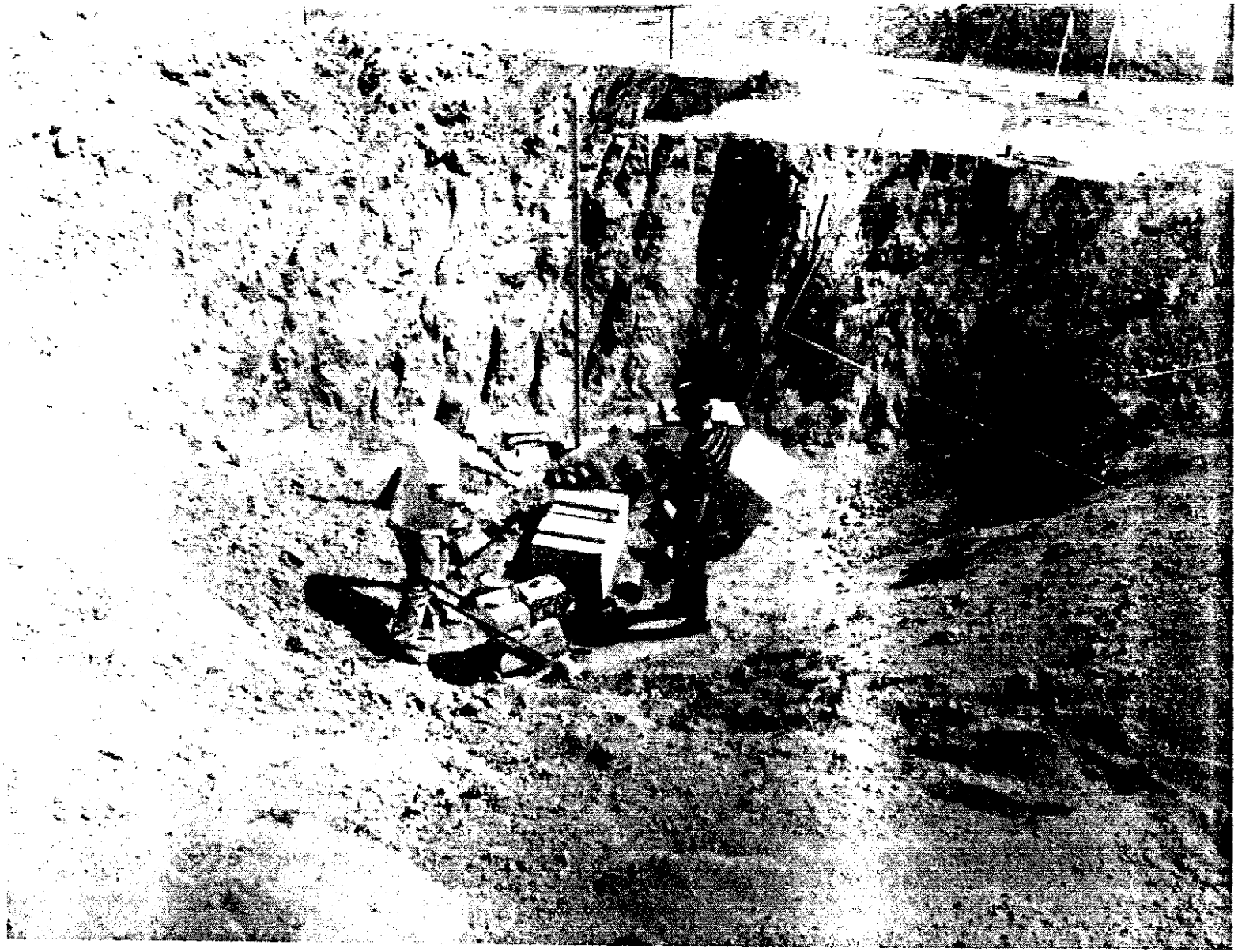

Figure 11. Cans and boxes placed in Test Pit 1, bottom layer (layer 4).

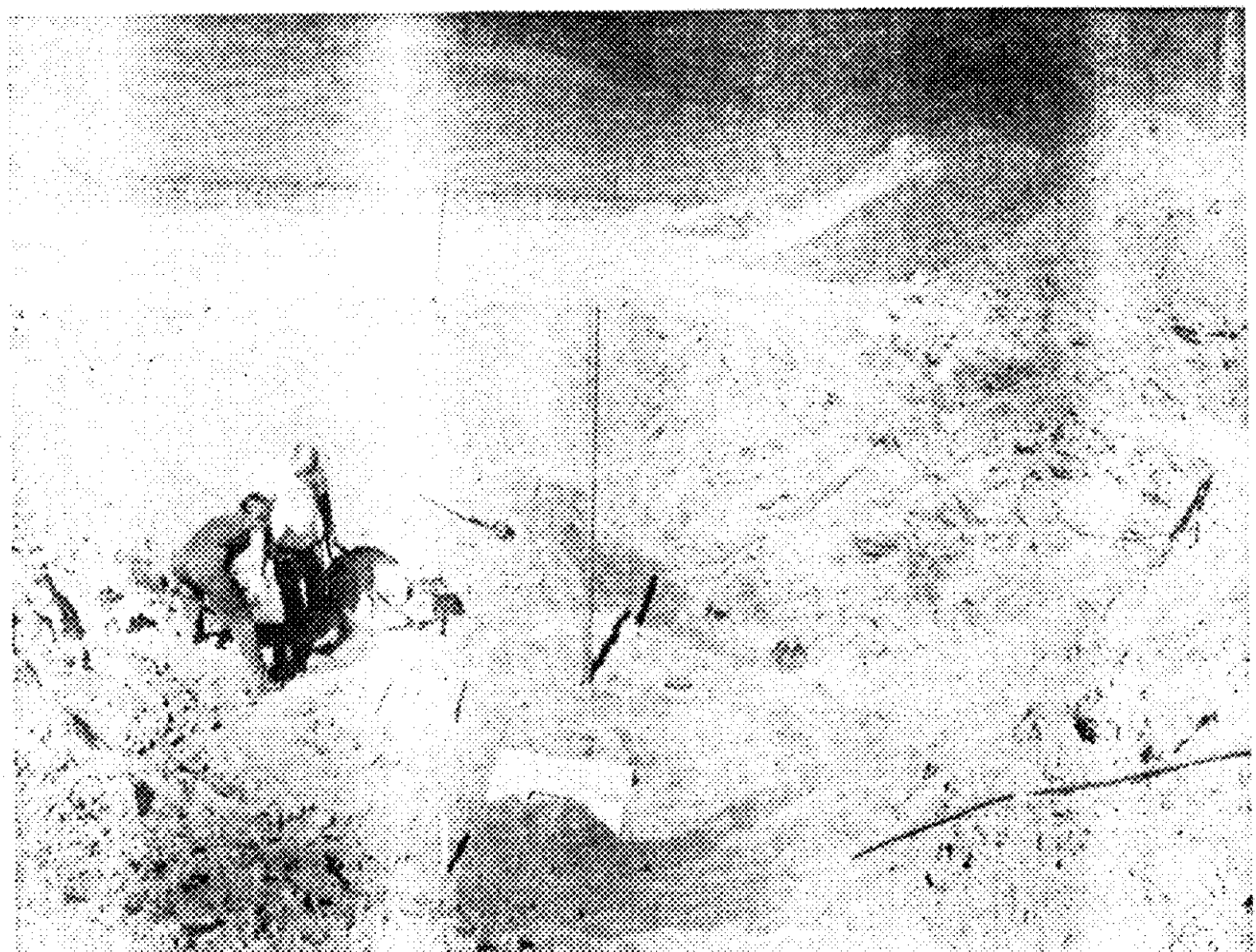

Figure 12. Test Pit 1 bottom layer covered with backfill.

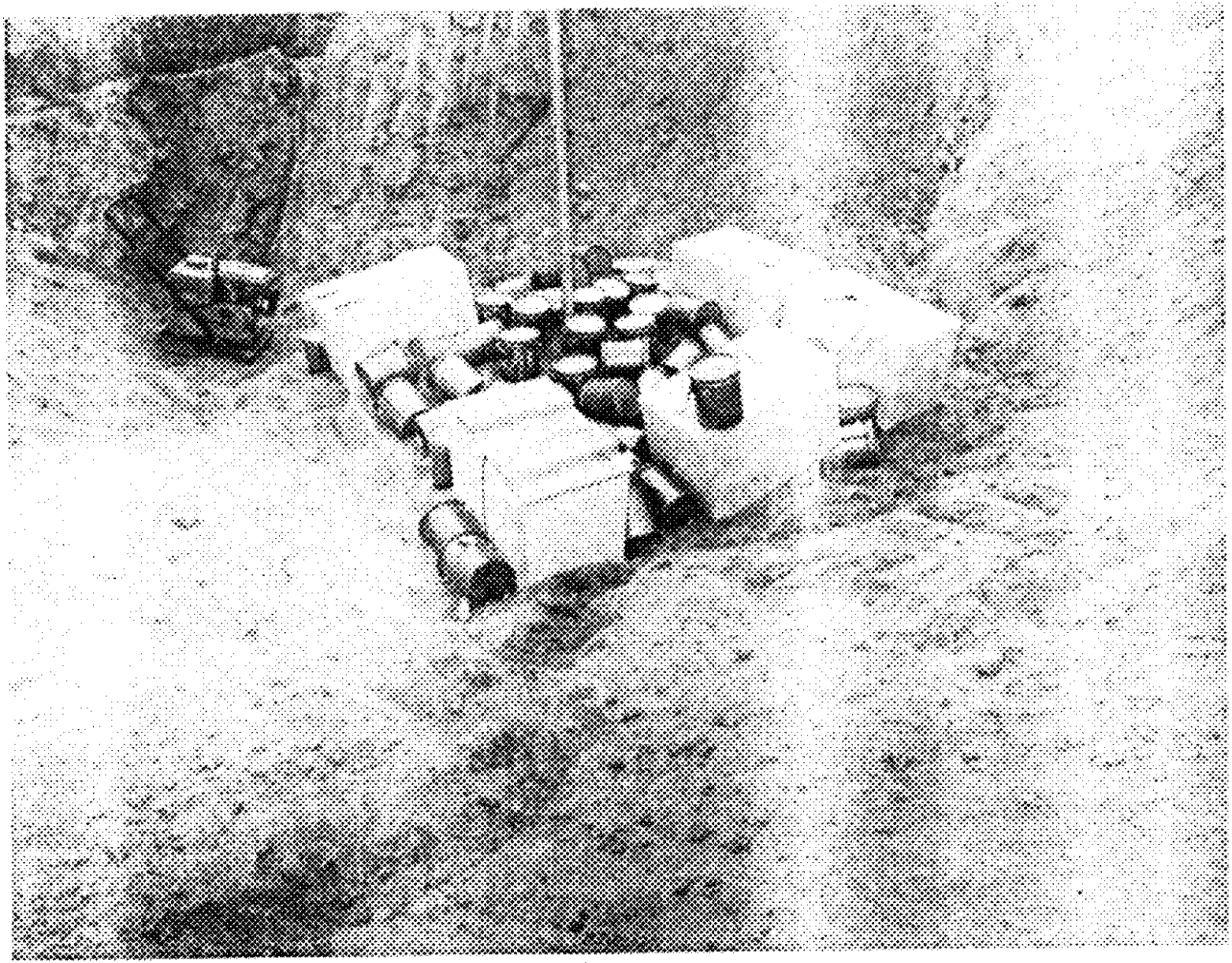

Figure 13. Cans, tracer cans contianing ytterbium oxide, and boxes placed in Test Pit 1, layer 2.

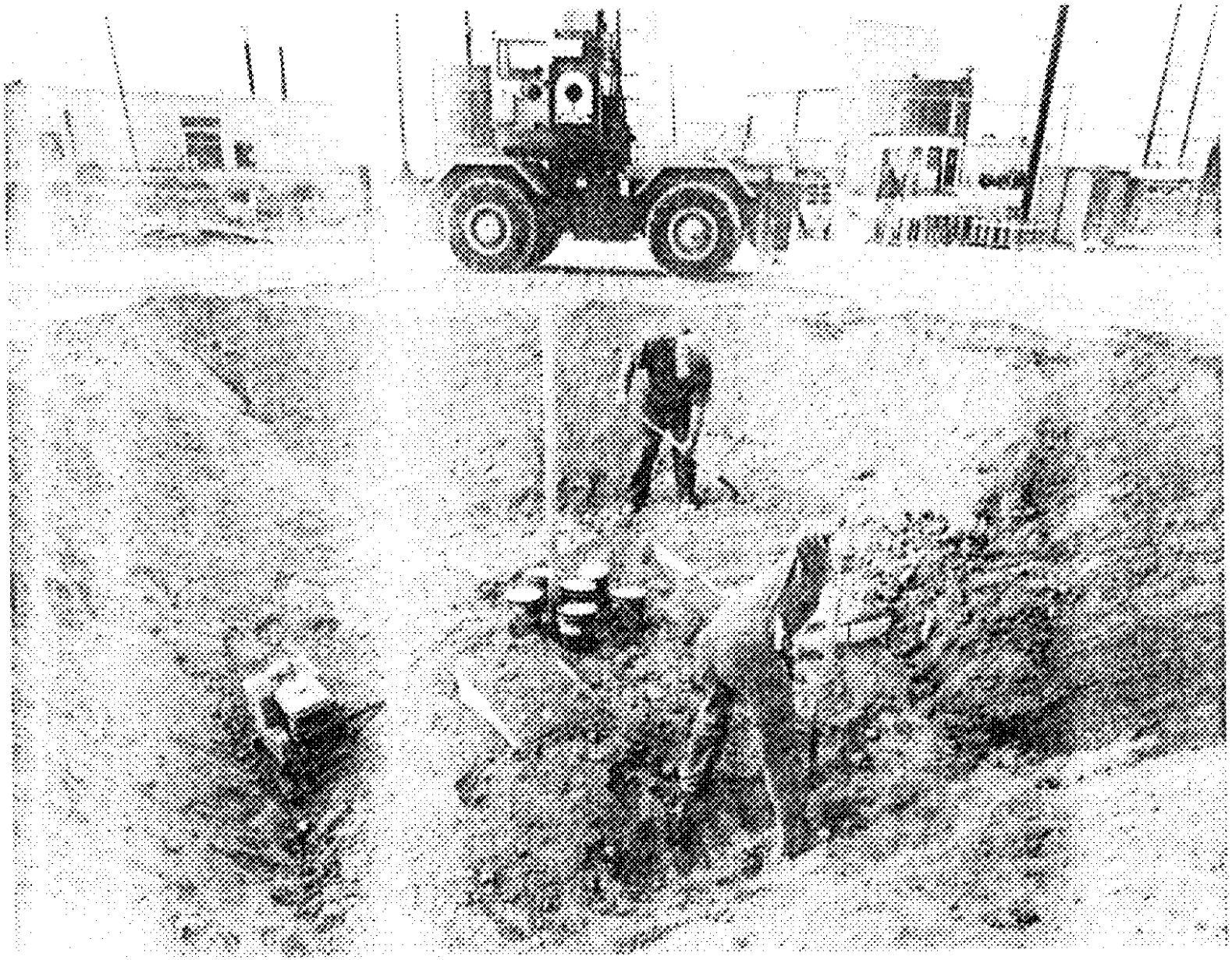

Figure 14. Backfill being placed over cans, tracer cans containing terbium oxides, and boxes in layer 2 of Test Pit 1.

Figure 15. Cans and boxes placed in Test Pit 1, top layer.

(6 in). A horizontal array was placed at approximately 1.4 m (4.5 ft) depth with thermocouples spaced 15.2 cm (6 in.) apart starting from the center of the pit. Unfortunately these thermocouples failed to perform during the test. The probable reason for failure was an unsuitable connecting wire leading from the thermocouples to the connection box at the process trailer. Part of this connecting wire was fiber braided and not coated with rubber. This was not suitable for outdoor use.

ISV testing on Test Pit 1 started October 18, 1989; however, hood failure occurred after approximately 14 hours of testing. As part of the accident investigation, a vitrified block approximately 48 cm (18 in.) deep was exhumed, and the soil overburden layer was excavated down to the tracer cans. The cans and the contents appeared unaffected by the melt. After excavation of the vitrified block, the soil overburden layer was replaced.

3.3 Test 1 Process Data Description

Test 1 operations were successful based on exceeding the target vitrification depth of 1.8 m (6 ft). This first field-scale test of a simulated buried waste site resulted in valuable operating experience and data relative to equipment design considerations and operating guidelines. As detailed later in this report, the information gained from Test 1 was utilized in Test 2 to improve operations. Generally, operations conducted on the random disposal orientation of Test 1 resulted in a very dynamic process that was extremely uncharacteristic of processing contaminated soil sites. Significant temperature and pressure spikes were observed in the hood throughout the test and appeared to be associated with each encounter of a buried can or box. Significant imbalances in the power supply routinely created electrical instabilities. Table 8 summarizes the sequence of events for the test.

Test 1 was initiated on June 12, 1990 at 1905 hours and had proceeded approximately 5 hours when a power cable in the Scott-Tee transformer failed. At that point a 46 to 51-cm (18 to 20-in.) layer of glass had formed with power at 103 kW. Operations were suspended for investigation, which revealed

Table 8. Test 1 - summary of events

Date	Time	Elapsed Time (hour)	Event
6/12/90	1905	0.0	Power to the electrodes.
6/13/90	0035	4.92	Transformer cable failure. Test aborted.
6/14/90	1546	-0.45	Data Acquisition System turned on.
6/14/90	1613	0.00	Power to electrodes. Restart initiated.
	1853	2.03	Melt resistance characteristics indicate melt is through starter path and into sand.
	2025	4.20	Tap change from 1000 to 650 V.
	2205	5.87	Average electrode depth 21 in.
	2215	6.03	Temperature and pressure spike noticed by operators. Electrode power reduced by operators.
	2301	6.80	Pressure/temperature spike. Hood made a loud "pop" sound. Smoke seen escaping through soil at base of hood, through air inlet HEPA, and around electrodes.
	2345	7.53	Pressure/temperature spike. "Bang" sound heard from hood. Resistance increased. Average electrode depth 25 in.
6/15/90	0000	7.78	Tap change from 650 to 1000 V.
	0021	8.13	Tap change from 1000 to 650 V.
	0033	8.33	Hood observation indicates flares and glass coming up around an electrode. Amperage dropping so tap change back to 1000 V tap.
	0120	9.12	Hood observation indicates glass shooting up vertically; yellow flares present.

Table 8. (continued)

Date	Time	Elapsed Time (hour)	Event
	0145	9.53	Pressure event. Amperage dropped 50% during event. Whole glass surface observed as molten with glass thrown 1.5-1.8 m (5-6 ft) in air. Large flames present.
	0320	11.12	Average electrode depth 34 in.
	0330	11.28	Power off to inspect cables around hood. Chunk of something (possibly wood) observed in melt, charred with ashes flaking off.
	0430	12.62	Average electrode depth 47 in.
	0523	13.17	Tap change back to 1000 V.
	0524	13.18	Sounds heard from within hood, cold cap disrupted by gas release and subsequently covered by molten glass.
	0550	13.62	Tap change from 1000 to 650 V.
	2650	14.62	Average electrode depth 60 in.
	0725	15.20	Tap change to 650 V.
	0830	16.28	Power off, transformer saturable core reactor fuses blown. All saturable core reactor fuses changed out. Electrodes stuck.
	0910	16.95	Power back on, using 650 V tap.
	0950	17.62	Transformer circuit breaker trip. Reset breaker. Electrodes gripped, no longer feeding by gravity alone. Electrodes still stuck.
	1000	17.78	Breaker trip. Reset.
	1010	17.95	Breaker trip. Reset.
	1020	18.12	Breaker trip. Reset.
	1022	18.15	Smoke from transformer, varistor failed, power off.

Table 8. (continued)

Date	Time	Elapsed Time (hour)	Event
	1100	18.78	Extension pieces to electrodes added.
	1155	19.70	Average electrode depth 71 in.
	1202	19.82	Power to electrodes for about 30 seconds, smoke from transformer, varistor failed.
	1405	21.87	Power back on, using 250 V tap. Electrodes are stuck, feed system cannot move them.
	1434	22.35	Tap change from 250 to 430 V. Phases not balanced. Phase B resistance is much higher than phase A.
	1450	22.62	Tap change from 430 to 650 V. Phases not balanced. Electrodes still stuck.
	1517	23.07	Power off to check fuses; they are OK. Power back on.
	1600	23.78	Average electrode depth 71 in.
	2220	30.12	Resistance of phase A increasing, power off, test terminated.

the cable received from the original manufacturer was undersized. A replacement cable was installed; all systems were inspected and tested; and preparations for restart were made, including relaying the starter path on top of the now frozen glass.

Test 1 was restarted at 16:13 hours on June 14, 1990. The power levels fluctuated during the test but generally averaged around 300 kW for the total test duration of approximately 18 hours and at the approximate total of 5400 kWh, as shown in Figure 16. Note that power is gradually increased over the first six hours to minimize possible disruptions in the starter path and to minimize the particulate generated by the oxidization of the graphite in the starter path. Hood plenum temperatures averaged around 300°C, which was slightly lower than predicted based on computer modeling. The lower-than-predicted temperatures were due to periods of nonpowered operations as a result of electrical imbalances associated with the power supply. Figure 17 illustrates the typical increase in resistance as the power distribution is transferred from the highly conductive starter path to the surrounding molten soil. As the molten soil zone grows, resistance decreases. The overall rate of downward melt growth averaged 4.6 cm/h (1.8 in./h), as illustrated in Figure 18. This average rate includes the final 15 hours of operation during which the downward melt growth rate was severely reduced due to the electrical imbalances described later in this report. The achieved melt depth was approximately 2.4 m (8 ft). Subsidence was measured at approximately 1.4 - 2.0 m (4.5 - 6.5 ft), leaving a 0.4 m (18 in.) layer of glass in the bottom of the vitrified area.

Gas releases from containers resulted in 14 separate events characterized by sharp temperature increases and/or pressure spikes in the hood. Many of these events also influenced other process off-gas components and the electrical system, as detailed in Section 3.3.2 (see p. 57). It is important to note that the pressure spikes were the result of either relatively slow gas releases from the melt or relatively slow expansions of gasses in the hood that occurred over a 10 to 30 second period. The pressure spikes were not rapid, which would be characteristic of a detonation or an explosion.

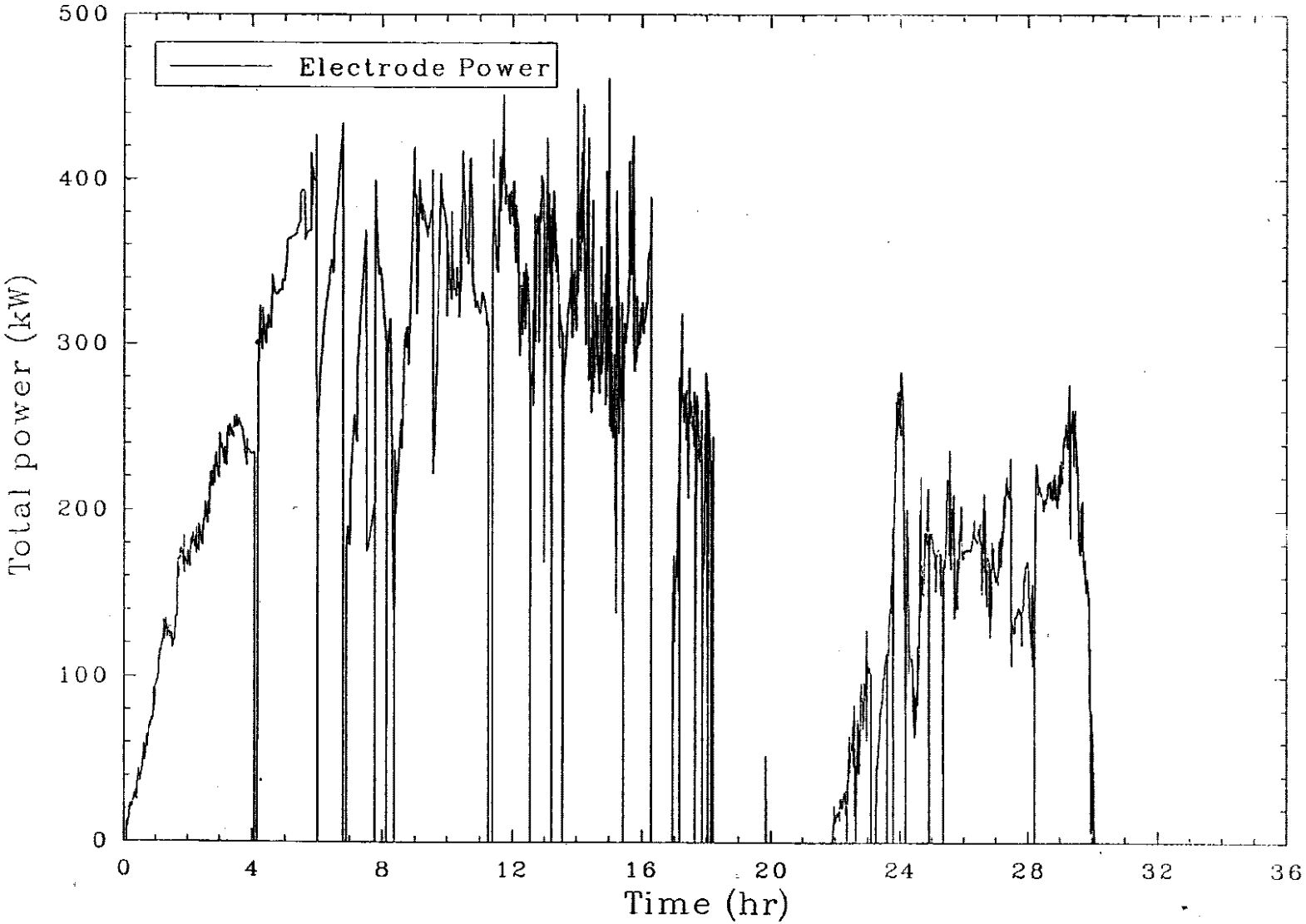

Figure 16. Total electrode power for Test 1.

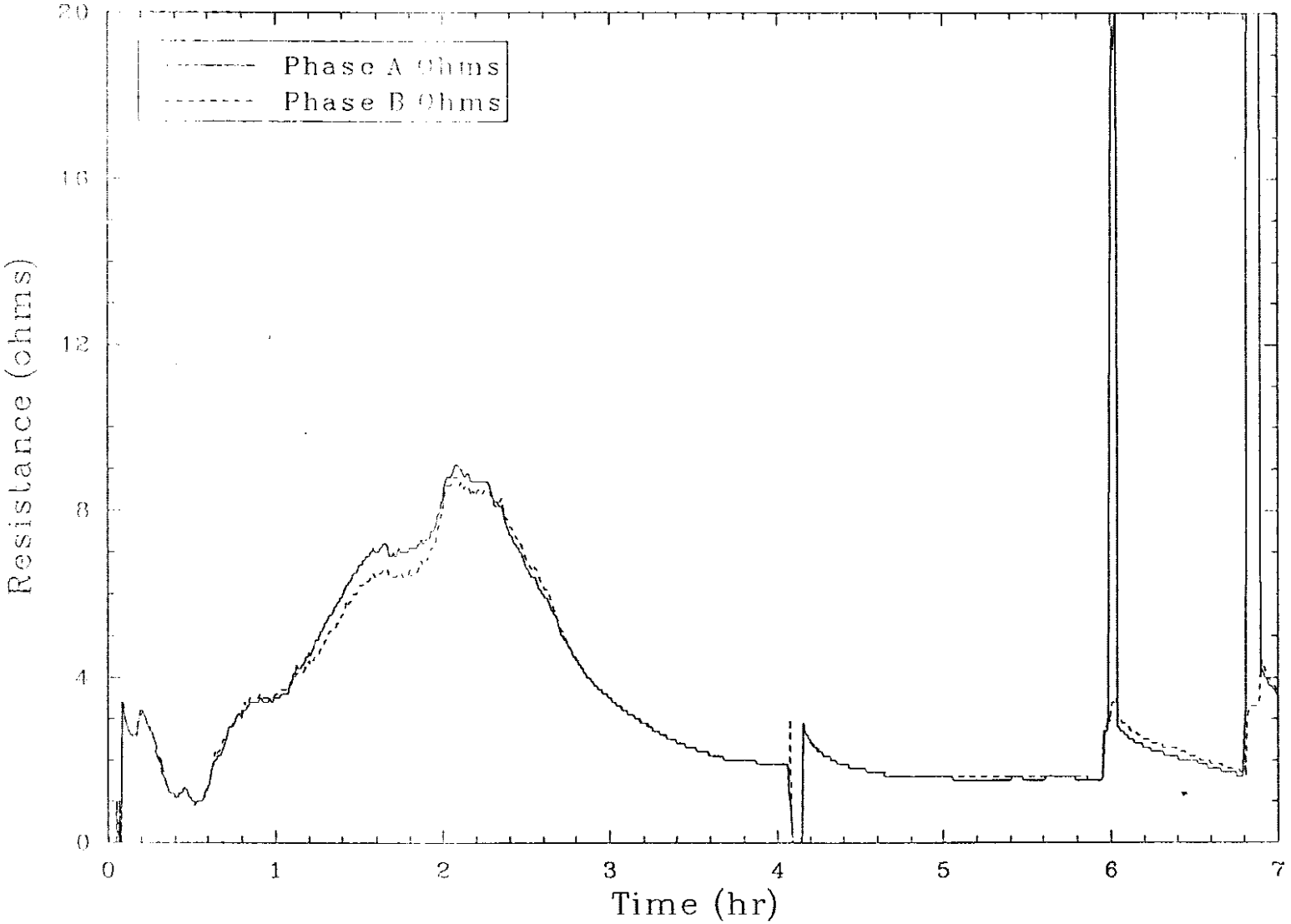

Figure 17. Phase resistance during startup for Test 1.

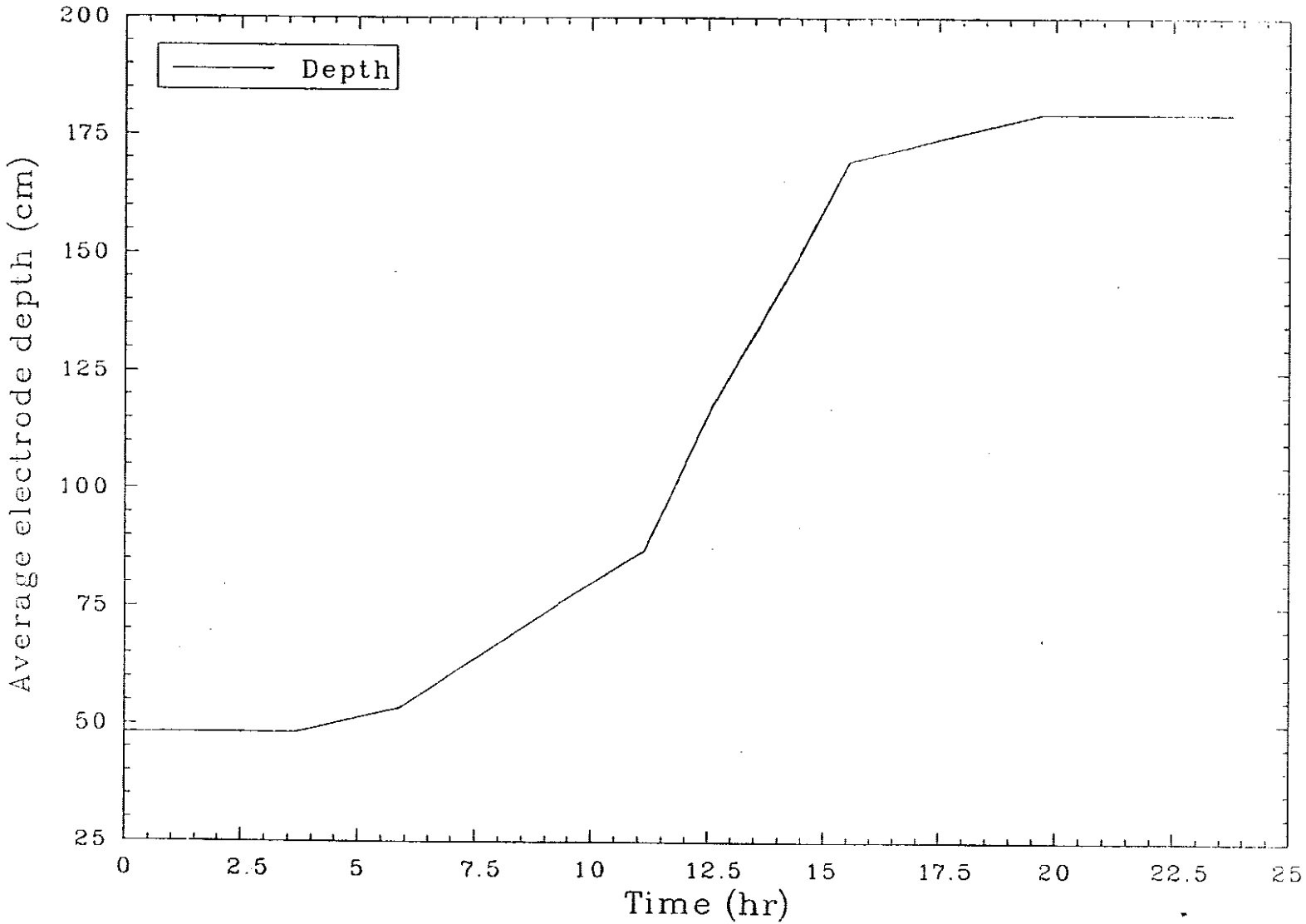

Figure 18. Average electrode depth for Test 1.

To fully analyze the ISV process operations and the behavior of buried waste processing, the following primary areas must be evaluated.

- Off-gas containment hood performance
- Power system and electrode performance
- Off-gas treatment system performance
- Off-gas system processing experiences
- Melt behavior at each event
- Electrical instabilities.

Note that the analysis of equipment performance is intended to serve as information supporting future design work for large-scale buried waste ISV processing systems.

3.3.1 Off-Gas Containment Hood Performance

The first intermediate-scale test of a simulated buried waste site resulted in a dynamic process, especially regarding conditions in the melt and off-gas hood. Surges in off-gas generation rates resulted in a loss of hood vacuum on several occasions; however, the hood was maintained at an overall average between 1.0 and 1.5 in. of water vacuum, and the plenum temperature maintained at an average of 300°C. Plots of the hood vacuum and the plenum temperature for the entire test are provided in Figures 19 and 20. A total of 14 significant temperature spikes were recorded, resulting in a net temperature increase ranging from approximately 50°C to over 300°C, as shown in Figure 20. The initial temperature spike in Figure 20 is biased high because this first event was observed to result in molten glass splashing up onto the tip of the plenum thermocouple. Other thermocouples in the hood suggest a true plenum temperature of approximately 700°C. The plenum temperature was generally the hottest temperature recorded in the hood because it is in the center of the hood cavity and was nearer to the molten glass than other thermocouples. Because the hood plenum thermocouple was not shielded from radiation, it is likely that radiant heat transfer was biasing these temperature values higher than true gas temperature. As shown in Figure 21, the cooler hood, roof, and wall temperatures parallel the plenum temperature.

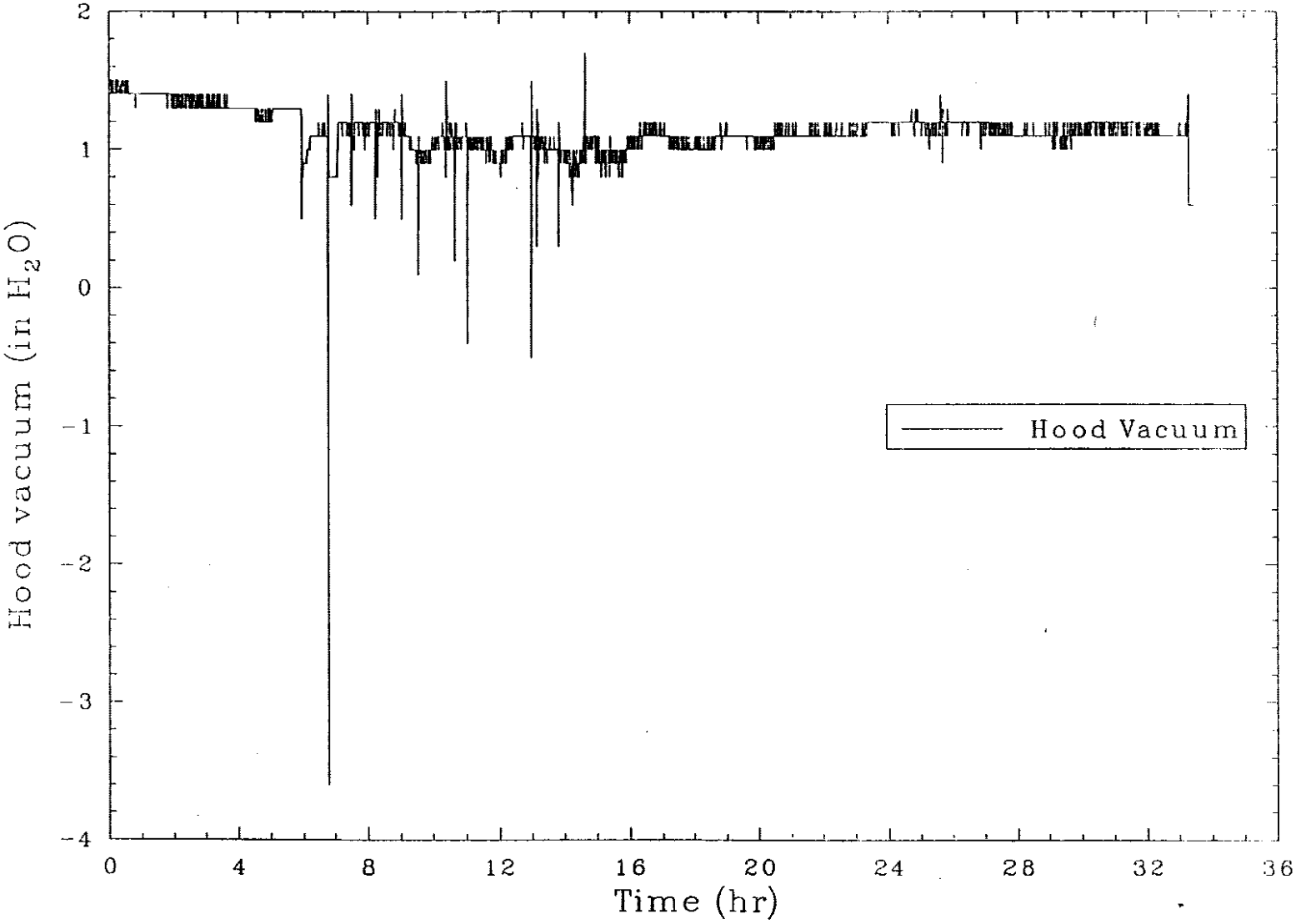

Figure 19. Hood vacuum plot showing pressure spikes for Test 1.

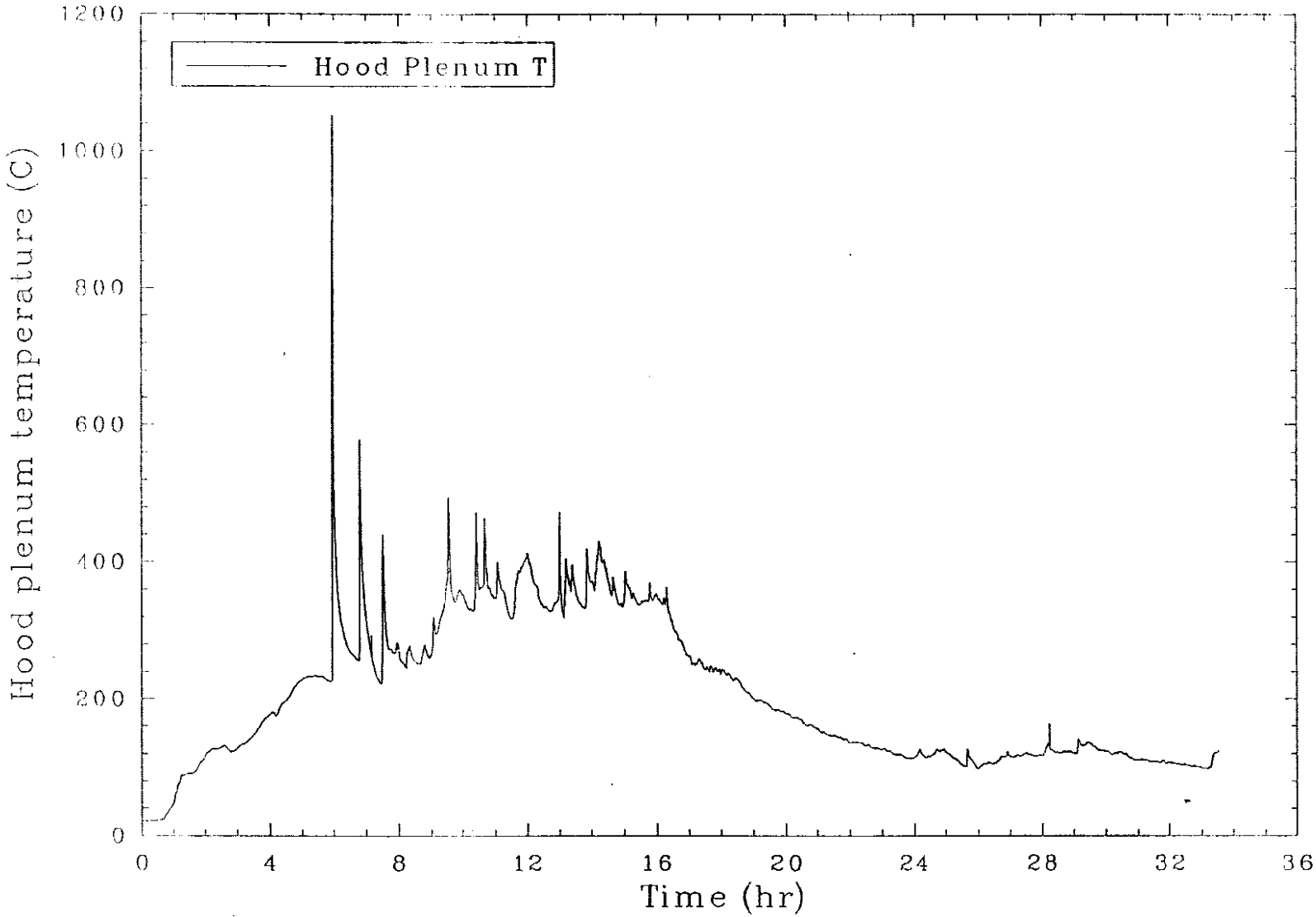

Figure 20. Hood plenum temperature plot showing temperature spikes for Test 1.

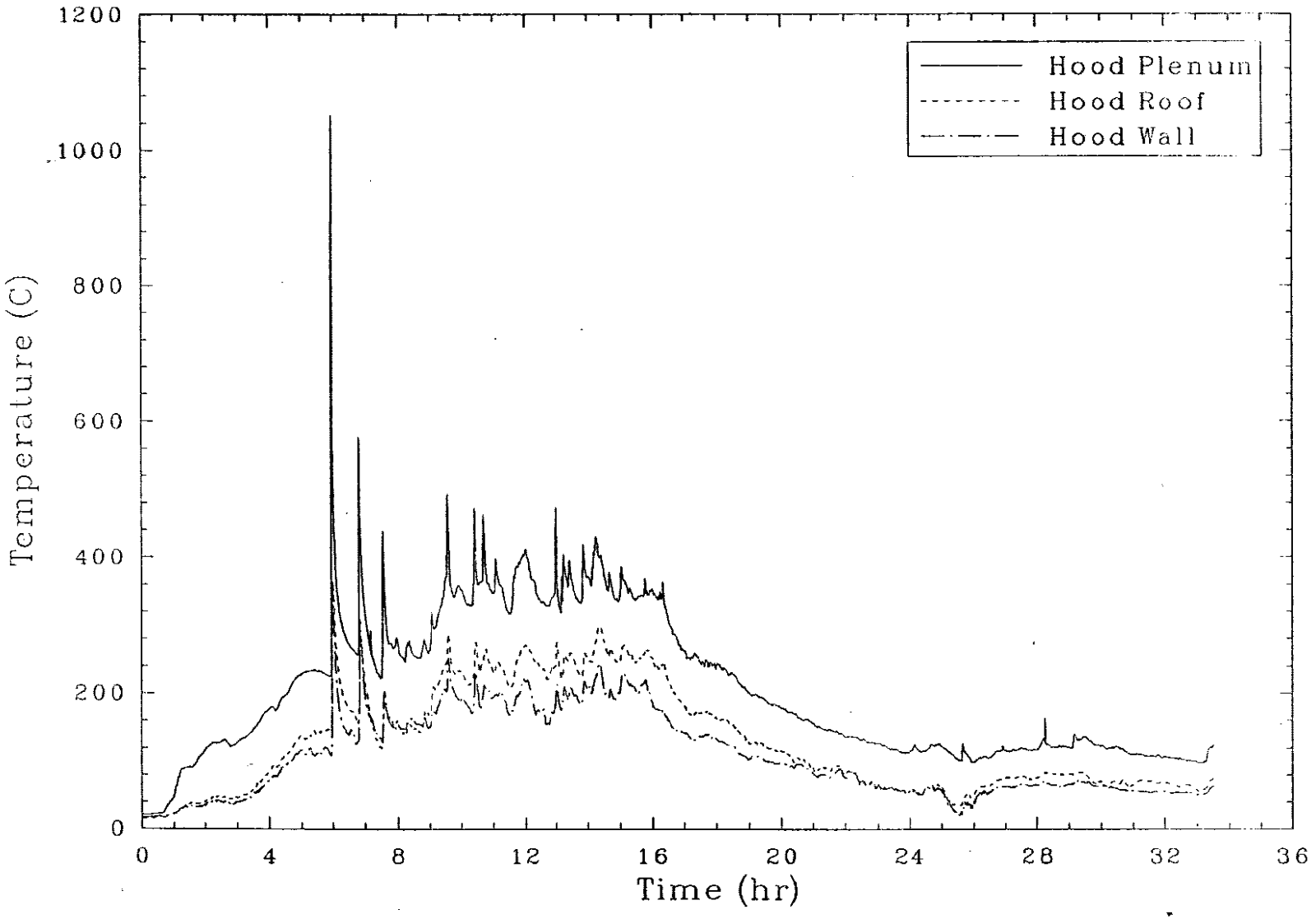

Figure 21. Hood Plenum, roof, and wall temperatures for Test 1.

Relative to the overall average processing temperature and temperature spikes, the off-gas hood performed as designed, maintaining its integrity throughout the test. On several occasions molten glass was ejected from the melt and contacted the hood containment panels, which resulted in significant localized heating. On at least two occasions during night operations, direct glass contact on the hood containment shell resulted in temporary localized heating that was observed by operators as a localized red glow. No significant thermally-induced structural degradations were observed following extensive examinations of the hood during and after the test. In addition, on several occasions, molten glass was ejected from the melt, contacting the high temperature fabric used for the electrode seals. This glass contact resulted in moderate degradation of the innermost layer, including a loss of structural strength due to partial melting of fibers. The outermost layers of fabric, however, were unaffected.

A high temperature sealant (RTV-106) was used as a test sealant compound for sealing some of the panel seams. The sealant remained pliant throughout the test and was used in locations on the containment hood that were directly exposed to the extreme temperatures inside the hood, as well as external seams that did not experience the extreme temperatures. Careful examinations following the test revealed no thermal degradation of the sealant on the external seams. Examinations of the internal seams revealed inconsequential surface degradation of the sealant that was directly exposed to the extreme temperatures to less than 1 mm (0.04 in.).

The intermediate-scale ISV system, appropriately sized for contaminated soil sites, was unable to contain transient pressure spikes in the containment hood on several occasions. This illustrates the need for a larger, more robust processing system for buried waste sites. These spikes were the result of relatively slow gas releases from containers, relatively slow gas generation created by the combustion of pyrolyzed products, and/or thermally induced expansions of existing gasses in the hood. The pressure spikes were not a sudden pressure spike characteristic of a detonation. Most pressure spikes occurred over a 10 to 30 second duration. In cases where the pressure in the hood did not exceed 1 in. of water, the gasses were contained within the surge volume in the hood and were subsequently drawn out to the process

off-gas treatment system. However, when pressures exceeded 1 in. of water, a portion of the gas was relieved through the HEPA filtered pressure relief system, with the balance being drawn through the off-gas treatment system. In extreme cases, when the pressure significantly exceeded 1 in. of water, the gas overcame the surge and pressure relief capacity of the hood and released through any available point including around the base of the hood and through unsealed panel seams. Figure 22 is a combined plot of temperature and vacuum versus run time. This plot illustrates the relationships between plenum temperature spikes and off-gas surges that resulted in sharp decreases in hood vacuum. As hot gasses are released from the melt and combust in the hood, temperatures in the hood increase. Additionally, as the gasses are released from the melt, the cold cap covering the molten glass is disrupted, resulting in a release of radiant heat to the hood. The resulting radiant heat loss from the molten glass causes the electrical resistance in the glass to increase. Figure 23 shows this effect for several gas release events.

3.3.2 Power System and Electrode Performance

The dynamic behavior of buried waste processing posed a variety of operational instabilities relative to the electrical power supply. As the melt encountered the buried containers, many of the sudden gas releases that affected the hood environment also affected the transformer. The primary cause for these disruptions was the minimal glass volume associated with the test. Inherent with any ISV process, the treated soil region is densified as water, soil gasses, and other decomposition products are driven off. This densification, or subsidence, typically ranges from 30 to 50% for a contaminated soil site. However, subsidence was significantly greater for this test (75%) involving a simulated buried waste site. It is expected that any buried waste site would result in at least 50% subsidence or greater primarily depending on the total void volumes and organic materials present.

Test 1 resulted in a total power level that varied typically between 300 and 400 kW. Plots showing amperage and volts for each phase are provided in Figures 24 and 25.

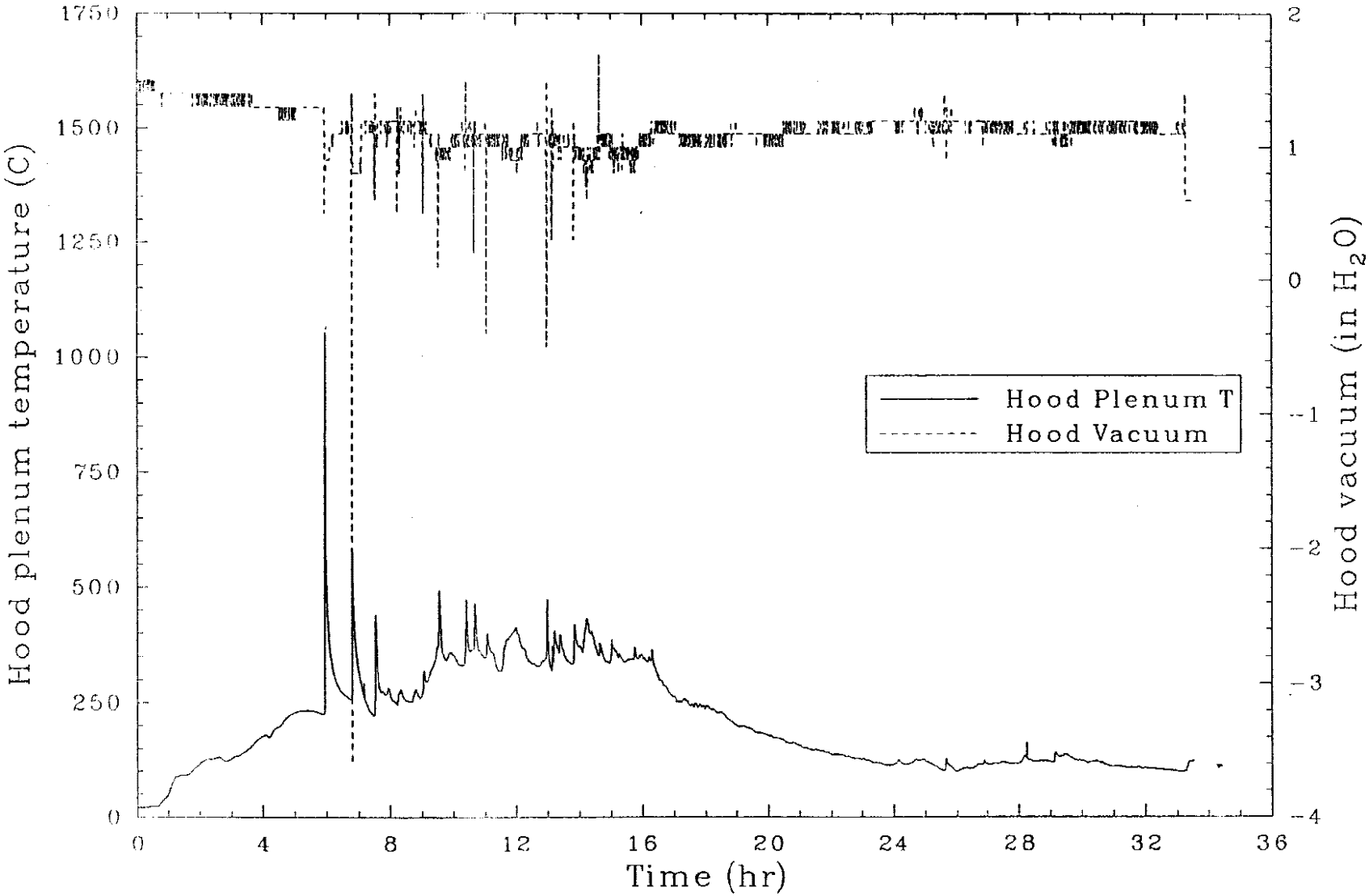

Figure 22. Hood vacuum and plenum temperature for Test 1.

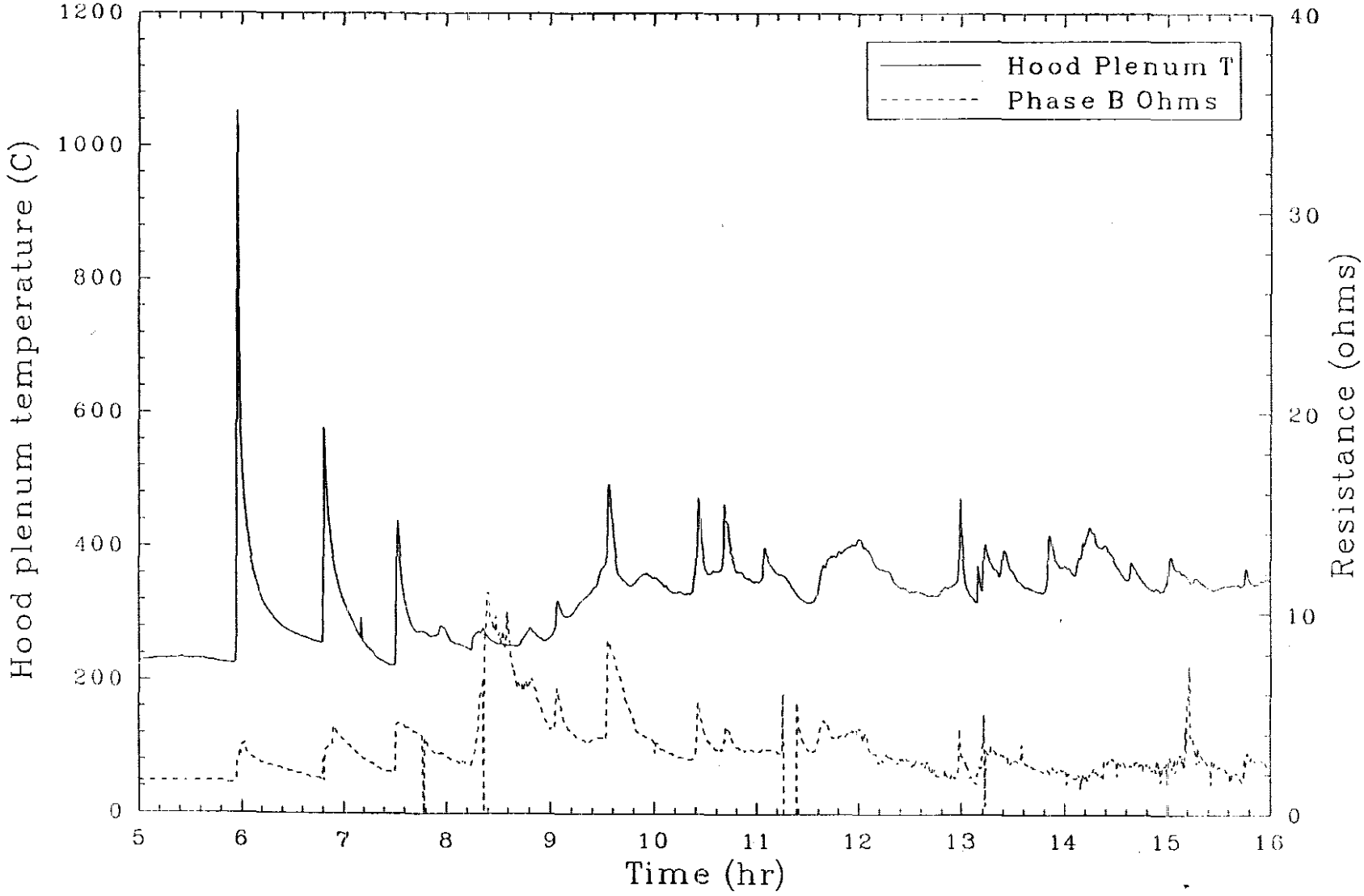

Figure 23. Hood plenum temperature and phase B resistance showing concurrent spiking in Test 1.

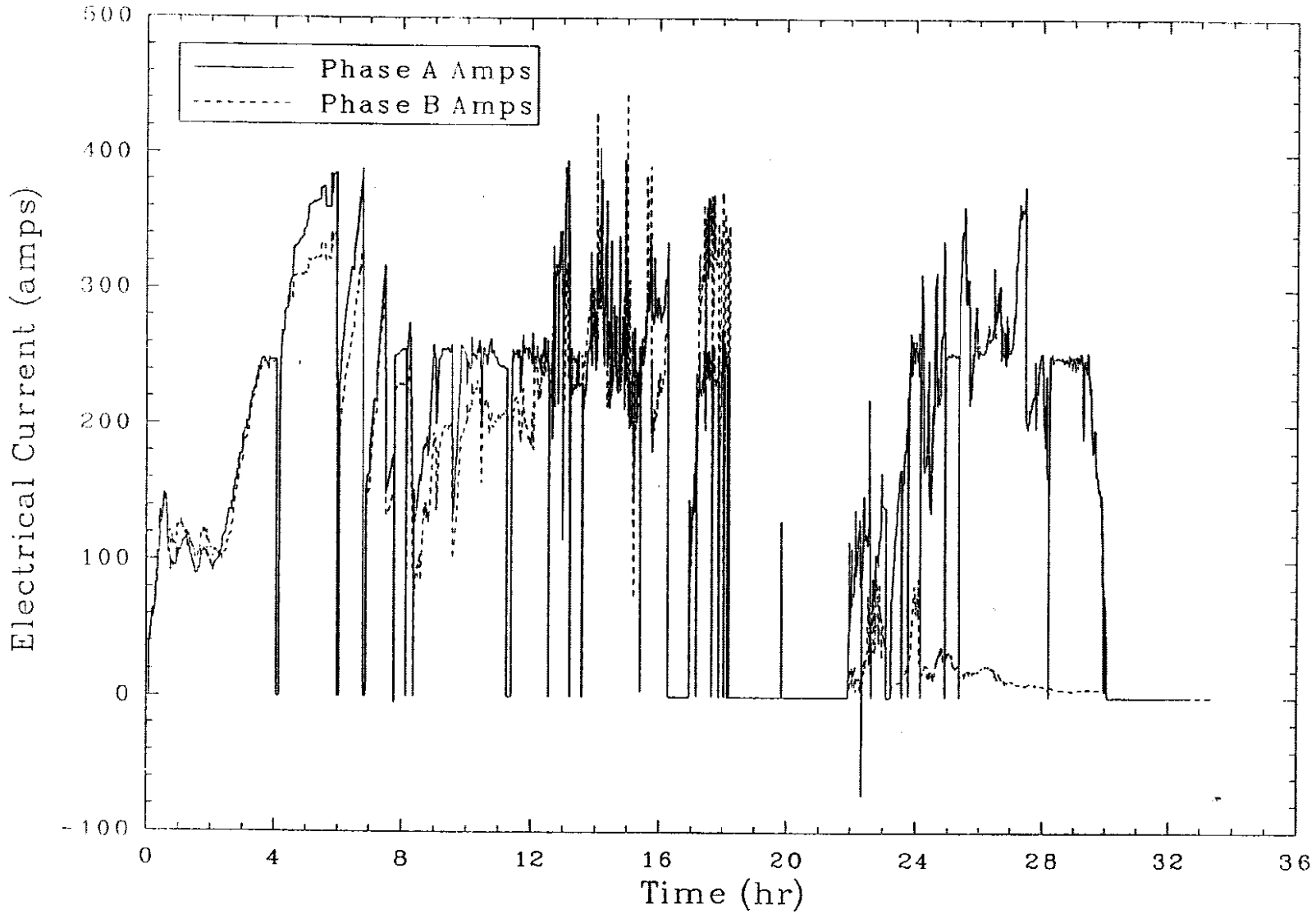

Figure 24. Phases A and B amperage for Test 1.

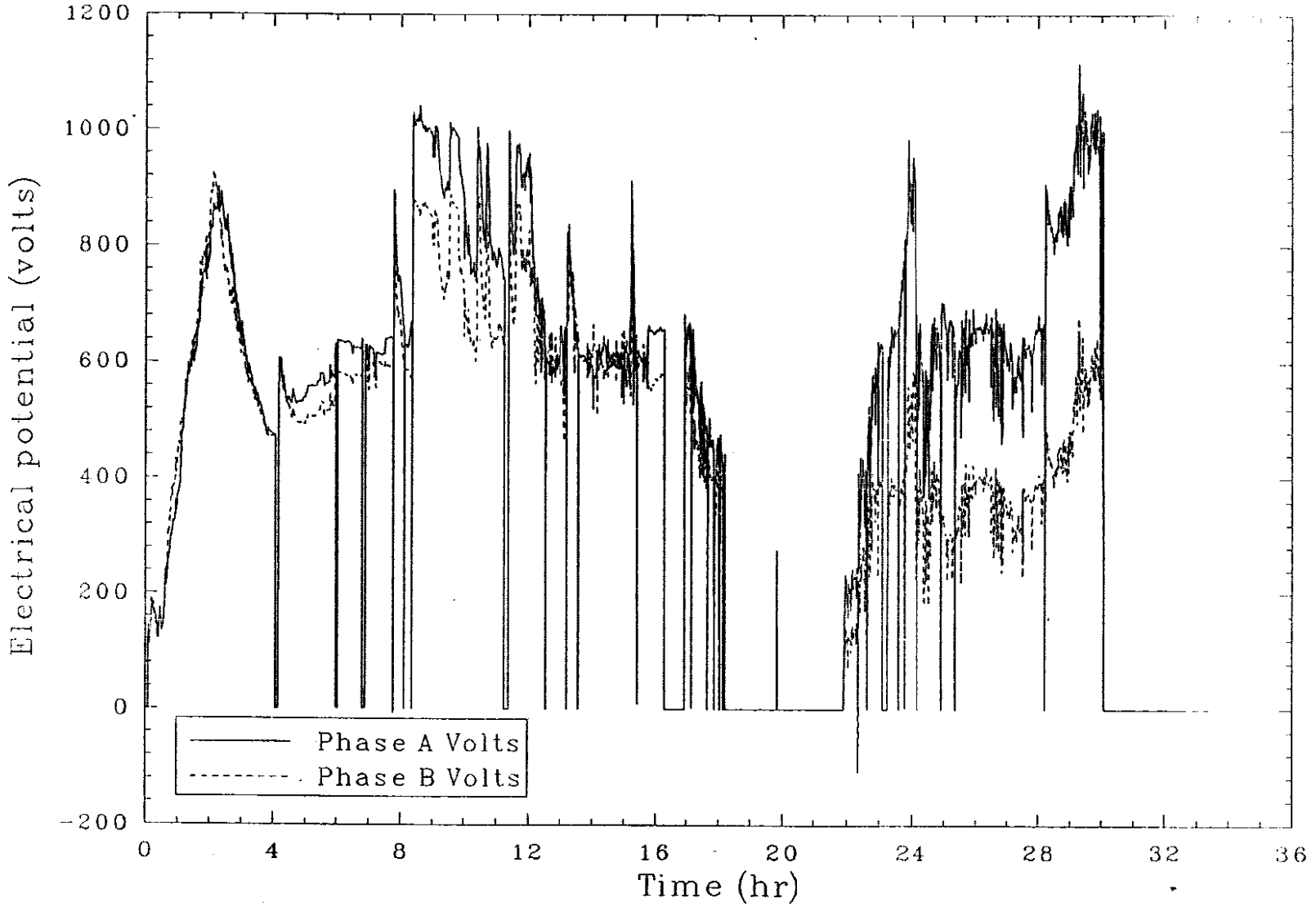

Figure 25. Phases A and B voltage for Test 1.

A minimal amount of glass available to the melt created electrical instabilities. For this test, only 0.61 m (2 ft) of soil overburden was available to provide a approximate 30 cm (12 in.) layer of glass before encountering the buried waste. As each waste container was encountered, glass would flow into the container, temporarily resulting in a net loss of glass between the electrodes available to conduct current. When containers near the edge of the melt were encountered, the glass would flow into the containers and freeze, thereafter being unavailable to the melt and resulting in a continual net loss of glass. With only a minimal level of glass to conduct the electrical current, the transformer was very susceptible to imbalances if one of the following conditions occurred.

- The electrodes were not inserted at an equal depth.

- Other nonelectrically conductive obstructions such as a partially dissolved waste container, a portion of the insulation blanket, ora piece of frozen glass dislodged from the cold cap, existed in the melt.

- Highly conductive objects, such as molten metal pools, created electrical short circuits between electrodes.

- Partially melted metallic objects contacting any of the electrodes effectively reduced the firing gap between the affected electrode and the opposing electrode.

- Sudden gas releases created electrically disruptive bubbles in the glass.

- Temporary localized area of cooled glass especially around an electrode resulted in increased resistance in that region. Glass cooling results from a cold cap disruption that allows molten glass to radiate heat to the hood environment. The radiant heat losses result in a net cooling of the molten glass in the localized area.

The resulting electrical instabilities appeared in a variety of forms and ultimately resulted in terminating the test shortly after the 1.8 m (6 ft) depth objective for the test was achieved. A key experience gained from this test involved the performance of the coating used to minimize oxidation of the graphite electrodes. Initially, the electrodes were painted with a silicon-based coating to help reduce oxidation. During ISV processing, the graphite electrodes tended to reduce in diameter at the air/melt interface due to the oxidation of graphite. The oxidation can lead to electrode failure if the electrodes are held in a static position for several hours. The use of the coating is a compromise in that, while the coating helps prevent oxidation, it tends to cause the electrodes to stick to the glass. Because this was the first field scale test of moveable graphite electrodes, it was determined that the use of the coating would be the prudent coarse of action. During the test, the electrodes became frozen to the cold cap and were unable to be moved (inserted or retracted) to compensate for electrical imbalances. The electrodes would become free from the cold cap whenever a container was encountered that disrupted or melted the cold cap with combustion or other sudden gas release and would free fall for typically 15 cm (6 in.) until they rested on the bottom of the melt. Ultimately, the test was terminated when the molten glass essentially melted away from the frozen electrodes during a period of time when no containers were encountered.

Electrical imbalances in the transformer resulted due to an unusually small volume of molten glass and the lack of electrode control caused by sticking. Because of the minimal glass volume, the effects of any transient condition in the melt was greatly magnified as compared to a situation involving several times the glass volume. For Test 1 the consequences of these problems included:

(a) 500 A saturable core reactor fuse failures due to imbalances on the primary side. Typically, operations for approximately 30 minutes in an imbalanced state of greater than 30% resulted in fuse failure.

(b) Thermal trips of the 750 A breaker to prevent overheating of the transformer. The excess heat was primarily caused by imbalances;

however, on a few occasions during the heat of the afternoon, the ambient conditions contributed significantly to the elevated transformer temperatures. The transformer automatically trips itself when temperatures in the secondary windings' approach 150°C above ambient.

c) Amperage limit trips or magnetic trips of the 750 A breaker due to the electrodes shorting in a metal pool. Although no absolute electrical shorts occurred during the test, on several conditions the presence of molten metal or metal objects near one or more electrodes created a higher than normal amperage situation. Those near shorting conditions were typically short-lived and affected only one of the two secondary phases. Due to rapidly changing conditions in the melt and the inability to respond with electrode movement (retract electrodes from a molten metal shorting condition), a resulting amperage spike would trip the transformer. Any imbalance on the primary side amplified the effect of this type of trip. Therefore, the imbalance combined with the near shorting condition resulted in magnetic or high amperage trips.

(d) Thyristor switch failures due to imbalances in combination with amperage surges. The surges do not necessarily have to be associated with an absolute metallic shorting condition. An absolute metallic short will occur when two electrodes are shorted via direct contact with a pool of molten metal or if a solid metallic object simultaneously contacted two electrodes. Limited amperage surges combined with an imbalance can cause failure of the switches. A limited amperage surge will occur if a single electrode contacts a molten metal pool or metallic object, effectively resulting in a shorter electrical pathway through the resistive glass to an adjacent electrode.

A key conclusion drawn from Test 1 is that the silicon-based coating causes unacceptable sticking of the electrodes to the cold cap. Due to the coating on the electrodes, the EFS was largely ineffective. All of the lifting force available (over 1500 lb) was insufficient to free the stuck

electrodes from the frozen glass. At one point, in the final hours of the test, an additional lifting force of 1000 lb was provided by a mobile crane; however, after determining the combined lifting force was insufficient to free the electrodes, the additional lifting force was terminated to prevent damage to the electrodes. Occasionally, a stuck electrode could be moved 1 to 2 cm (0.4 to 0.8 in.) up or down, but the electrode would not break free.

Aside from being stuck in the glass due to the coating, the graphite electrodes performed satisfactorily. Oxidative losses on the four electrodes were negligible. This test likely represented a near worst case condition for the electrodes because the location of the air/glass interface relative to the electrode did not change significantly throughout the test. In typical operations, the electrode is inserted at a rate that exceeds the rate of subsidence. Therefore, the electrode area most susceptible to oxidative losses is always replenished by feeding (inserting) more electrode from above. Based on these results, electrodes would not be coated for Test 2. In addition, a deeper layer of cover soil would be added to increase the volume of molten glass to help reduce electrical instabilities.

3.3.3 Off-Gas Treatment System Performance

The first field test using ISV on a simulated buried waste site resulted in a dynamic process. As each container was encountered by the advancing melt front, the changes created by gaseous releases that affected the hood environment and transformer also affected the process off-gas treatment system. Overall, the off-gas treatment system performed well.

The performance of the Venturi-Ejector relative to heat removal is illustrated in Figure 26, which shows the gas temperature entering the Venturi-Ejector typically ranged from 200 to 300°C. The exit temperature (Hydro-Sonic entrance) was typically less than 50°C. Fluctuations in differential pressure for the Venturi-Ejector, shown in Figure 27, were due to corresponding hood vacuum fluctuations. The pressure on the upstream side of the Venturi-Ejector was measured on the off-gas line that was directly affected by fluctuating hood vacuums.

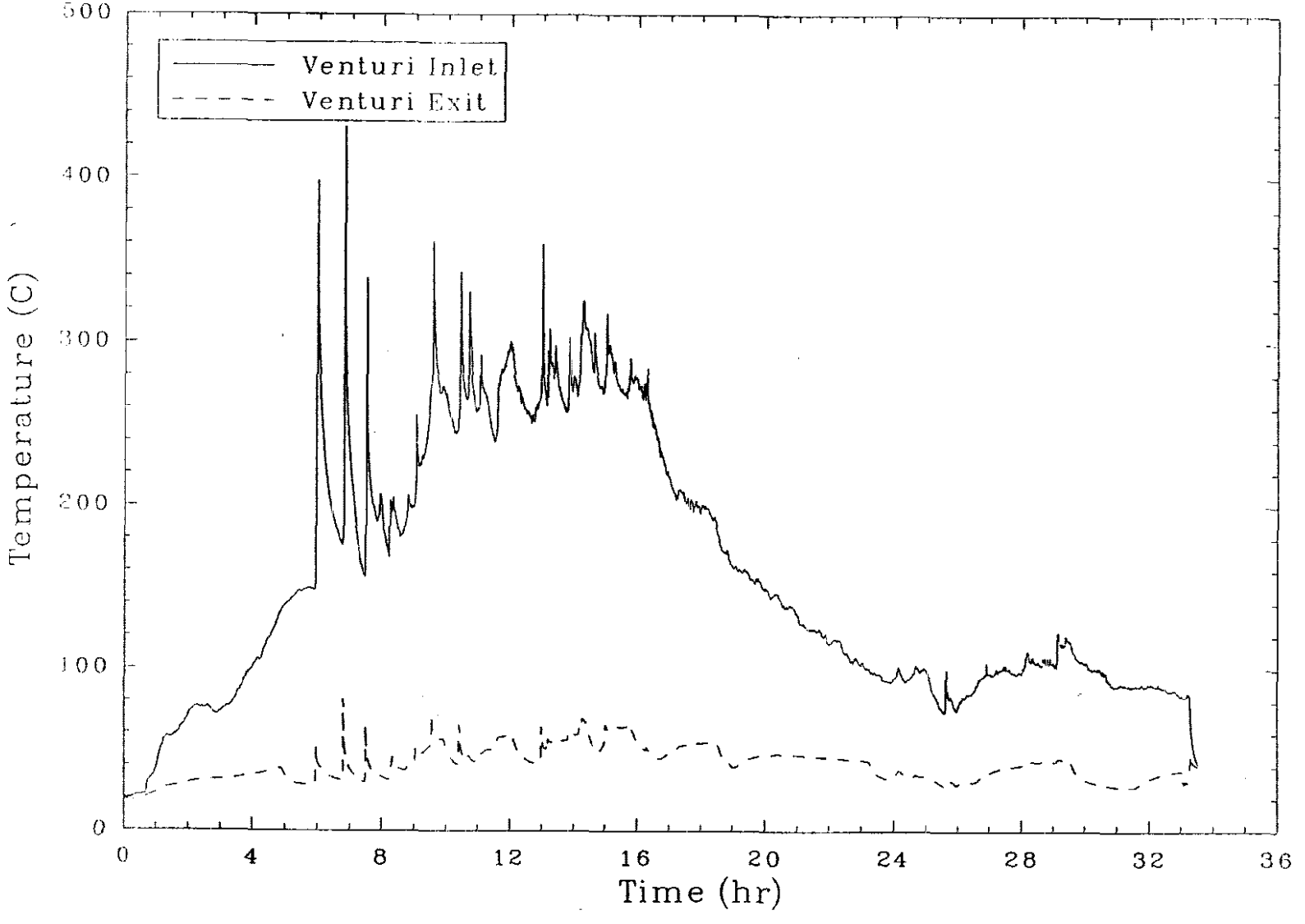

Figure 26. Temperature at inlet (off-gas at trailer) and exit of Venturi-Ejector for Test 1.

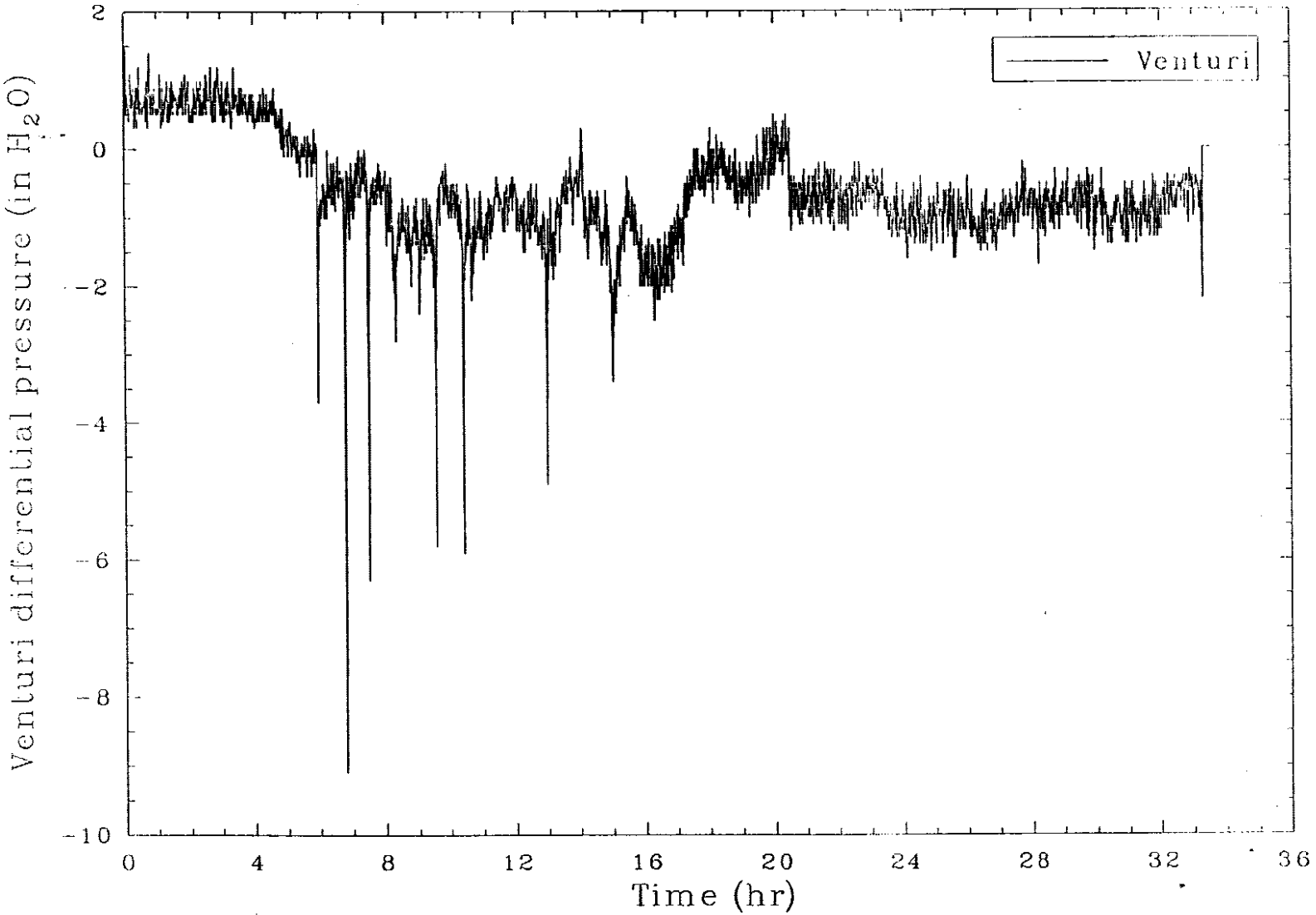

Figure 27. Venturi-Ejector differential pressure for Test 1.

The Hydro-Sonic scrubber differential pressure was maintained well above 50 in. of water throughout the test, as shown in Figure 28. By design, this should have resulted in a particulate removal efficiency of greater than 90% for particles sized greater than 0.5 μ. The fluctuations of differential pressure were due to fluctuations in total off-gas flow created by the automatic adjustment of the blower surge protection valve.

Differential pressure measured across the housing of the primary HEPA filter is shown in Figure 29. The differential pressure remained relatively constant throughout the test, indicating the scrubbers effectively removed the vast majority of particulate. Thus, a large-scale machine with a wet scrubbing system of comparable design could sufficiently remove particulate from the off-gas stream.

Total gas flow through the off-gas treatment system is shown in Figure 30. Total flow ranged from 12 to 22 m^3/min; however, periods where total off-gas flow exceeded 20 m^3/min coincided with the blower surge protection valve being opened, resulting in a false high reading. Later in the test, after 20 hours, off-gassing from the melt decreased due to the lower power input related to transformer imbalances. At the time the off-gas system was shut-down (approximately 3 hours after electrode power was terminated), the off-gas flow had decreased to approximately 12 m^3/min. Because off-gassing from the melt at this point in time would have ceased, this flow rate is largely the controlled in-leakage of air into the hood.

Concentrations of oxygen and carbon monoxide were monitored at the off-gas stack throughout the test. The oxygen concentration averaged between 20 and 21%, as can be seen in Figure 31. Short periods of reduced oxygen concentrations were measure at time periods consistent with gas releases from containers. This was consistent with the combustion of gasses in the hood upon release from containers in the melt. Carbon monoxide concentrations at the stack fluctuated throughout the test corresponding to gas releases from the containers in the melt and combustion activity in the hood. As shown in Figure 32, carbon monoxide concentrations ranged from 0.1 to 0.4%, with occasional spikes greater than 0.4%, up to a maximum of 1.1% at startup. The greatest concentrations of carbon monoxide are expected shortly after startup

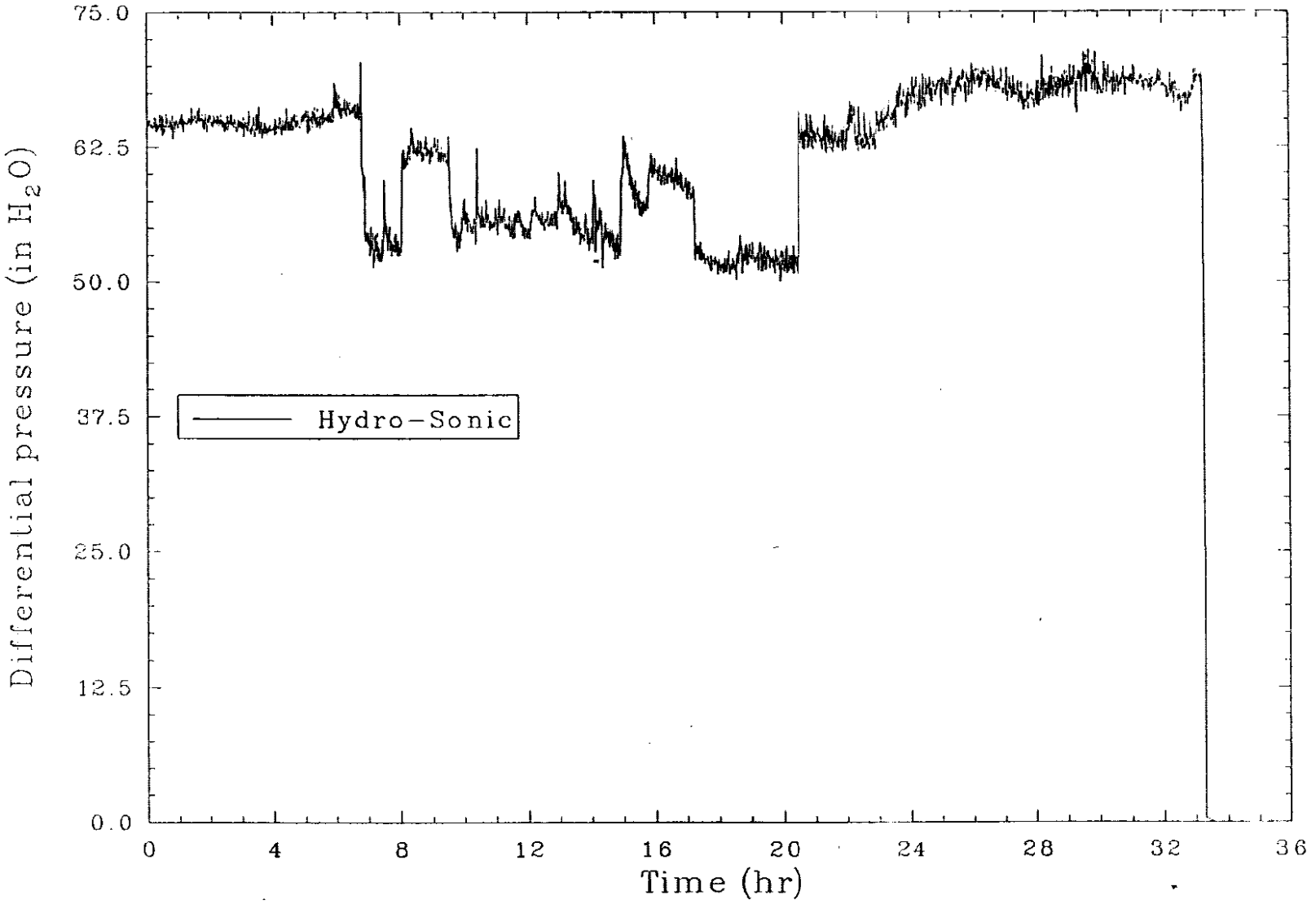

Figure 28. Hydro-Sonic scrubber differential pressure for Test 1.

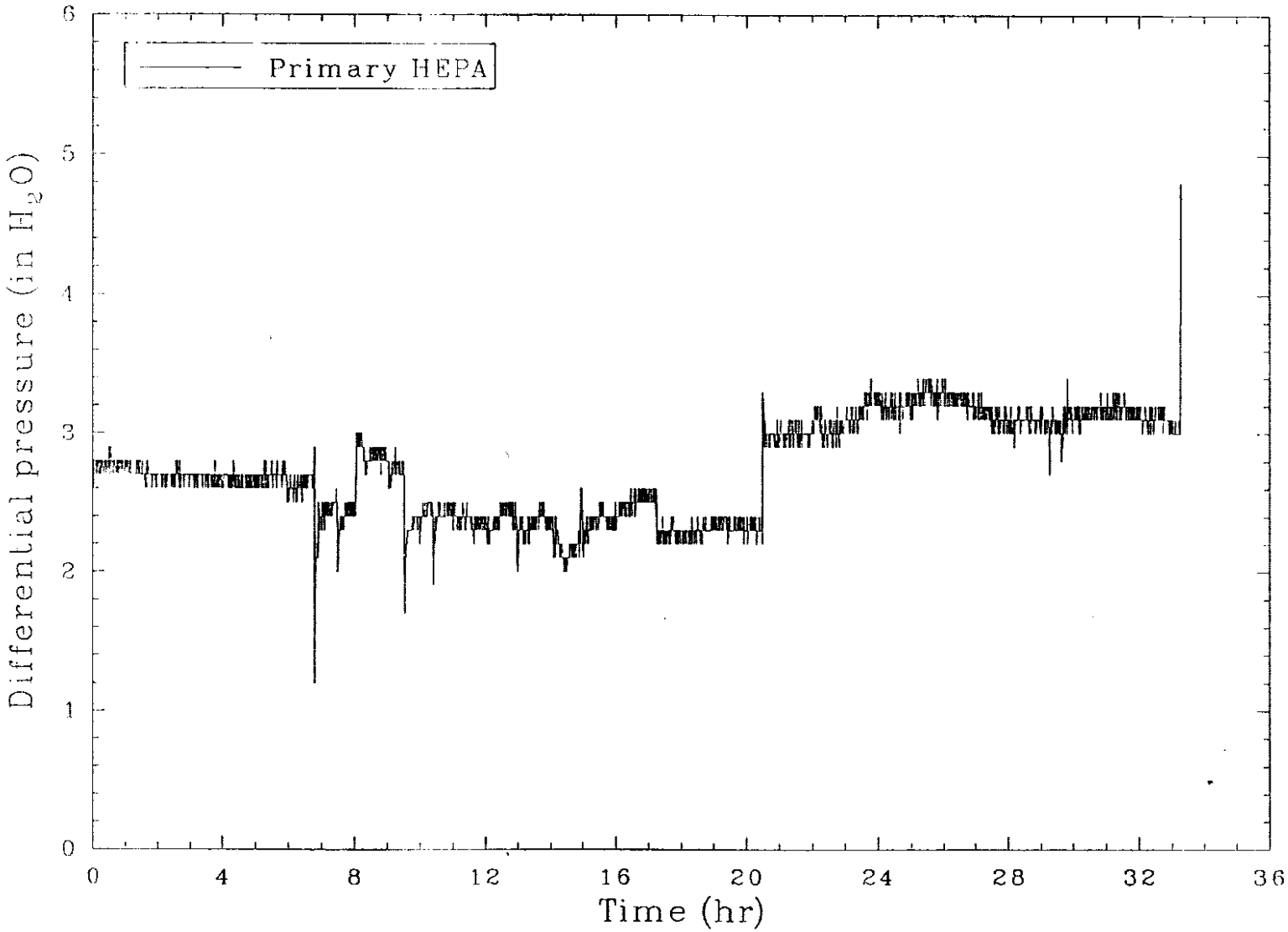

Figure 29. Primary HEPA differential pressure for Test 1.

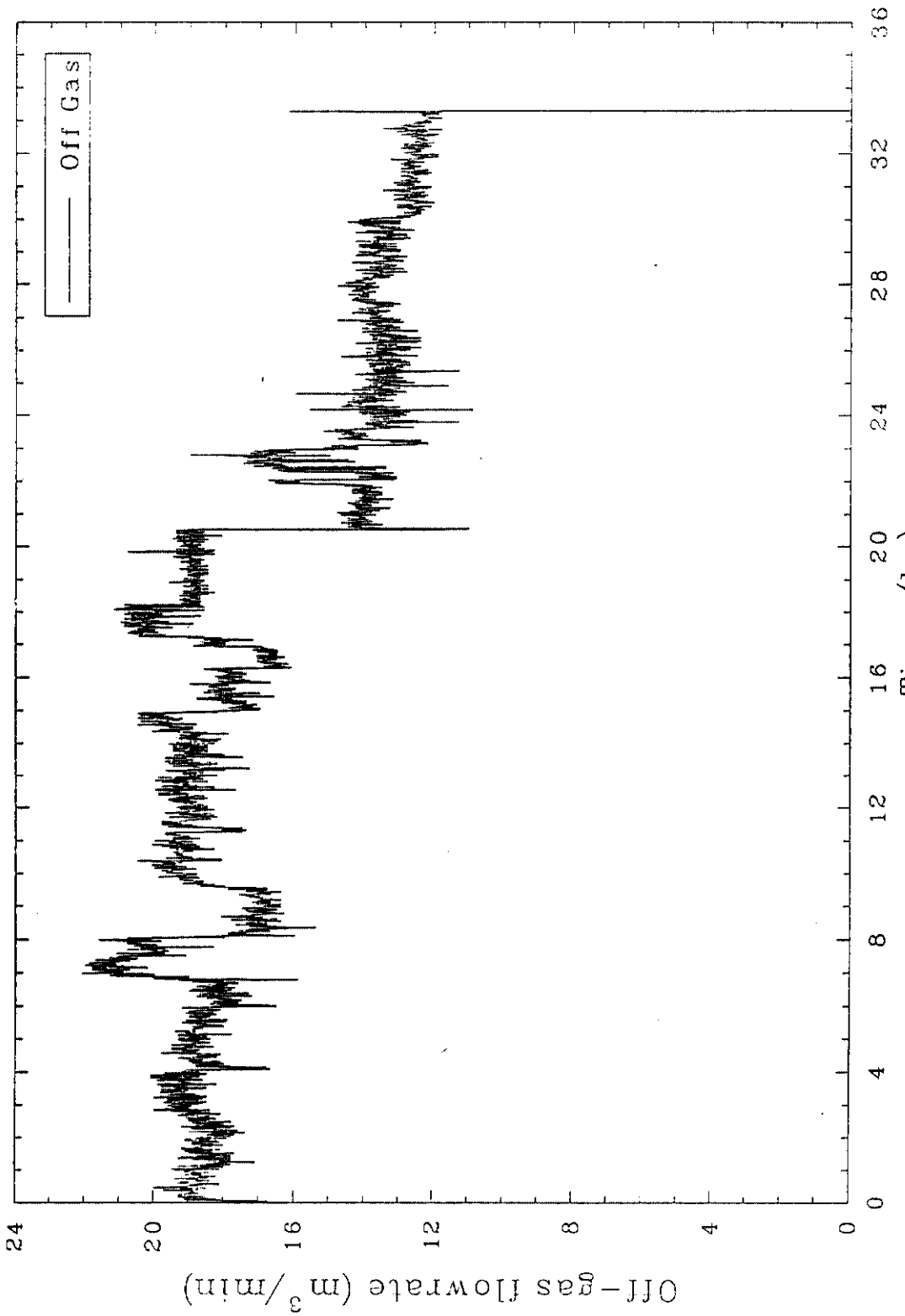

Figure 30. Total off-gas flow rate for Test 1.

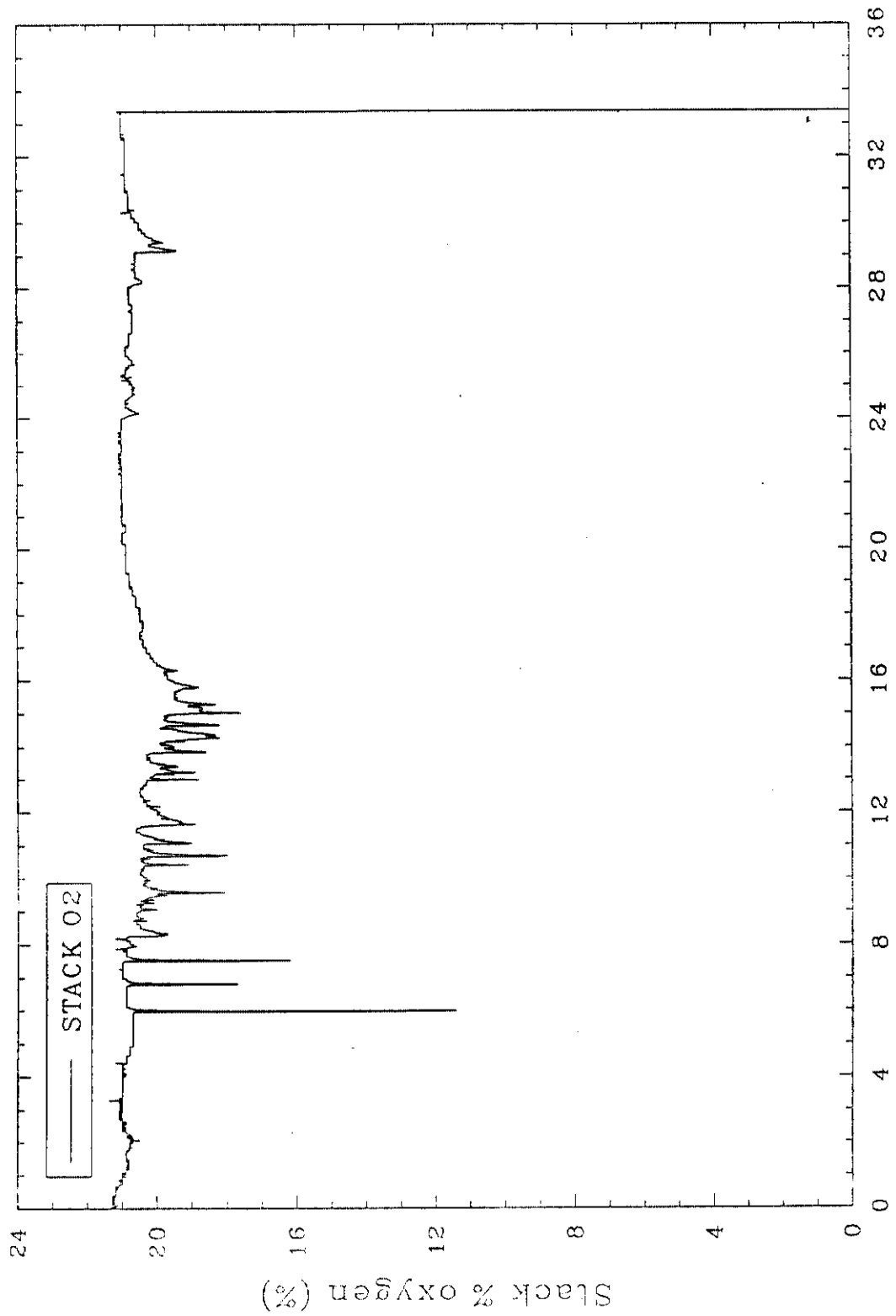

Figure 31. Stack oxygen concentration for Test 1.

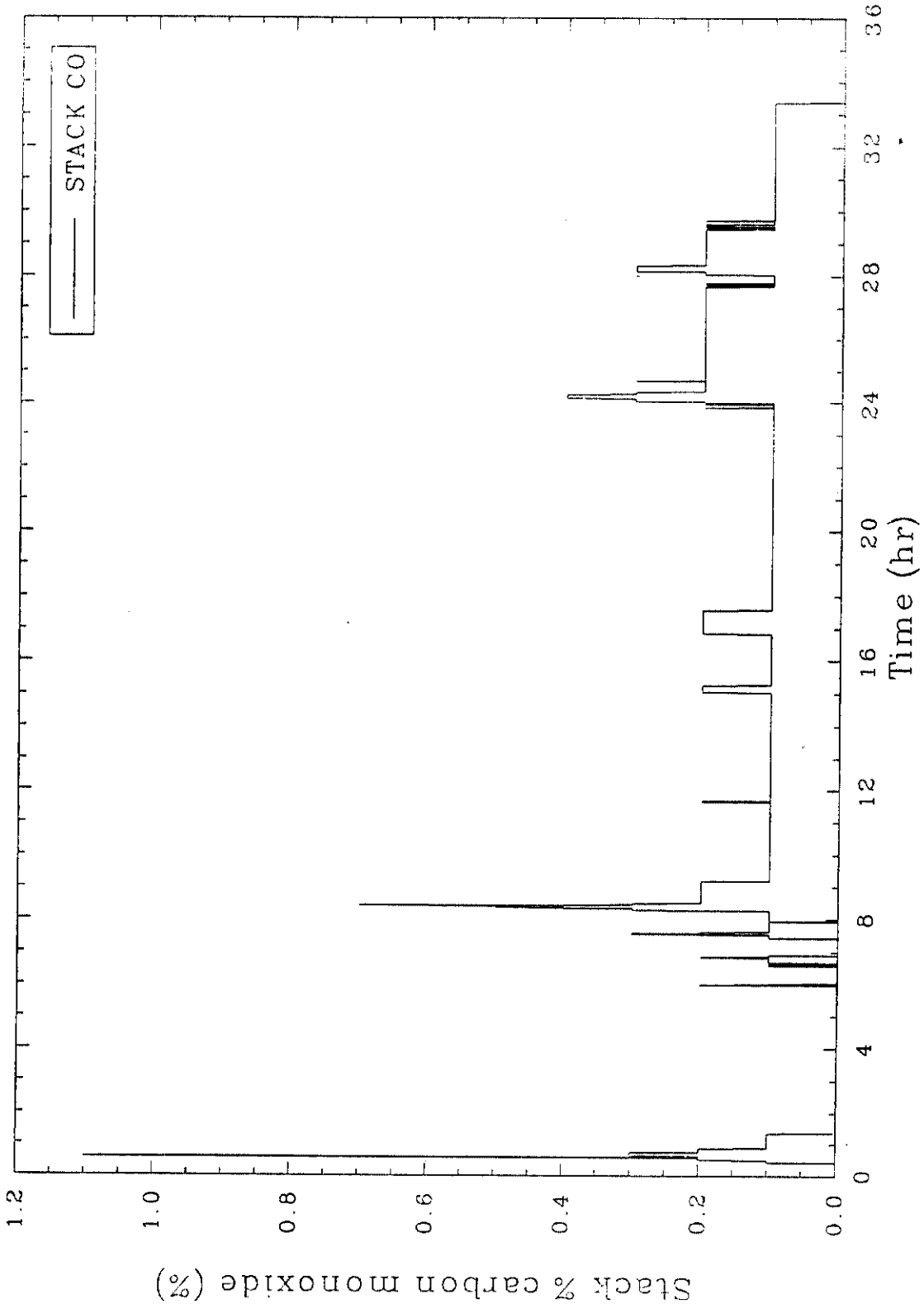

Figure 32. Stack carbon monoxide concentration for Test 1.

as the graphite starter path is consumed. Several pressure spikes resulted in a slight decrease in the oxygen concentration but were not accompanied by increases in carbon monoxide, as shown in Figure 33. It follows that the gas release from the melt in those cases was due to a release of steam or other noncombustible gas from a container, such as the noncombustible sludge cans that contained water. This phenomenon is explained by the release of noncombustible gasses from the melt, such as steam effectively displacing or decreasing the quantity of air entering the hood.

3.3.4 Off-Gas System Processing Experiences

The processing of the simulated buried waste site resulted in unusual off-gas processing equipment behavior and operating conditions relative to ISV processing of a contaminated soil site. The frequent temperature and vacuum fluctuations in the hood resulted in several operational consequences that appeared to be characteristic of processing any buried waste site. The key observations for Test 1 relative to the operation of the off-gas treatment system are summarized below.

- Increased melt rates resulted in more water vapor being introduced to the process off-gas system. As the melt progressed, water vapor in the soil was driven off as steam and condensed in the off-gas treatment system. With an increased melt rate, such as that seen in Test 1, the corresponding increased rate of water removal to the off-gas treatment system challenged the evaporative capability of the off-gas system. Consequently, the process scrub tank temperatures were operated near the maximum design limits to increase evaporative losses. It is important to try to maintain a water balance in the scrub solution tanks to prevent the undesired accumulation resulting in an increase in the secondary waste stream. This situation will result regardless of scale. Consequently, large-scale machines designed to process buried waste sites will require an improved evaporative capability to minimize the generation of secondary liquid wastes.

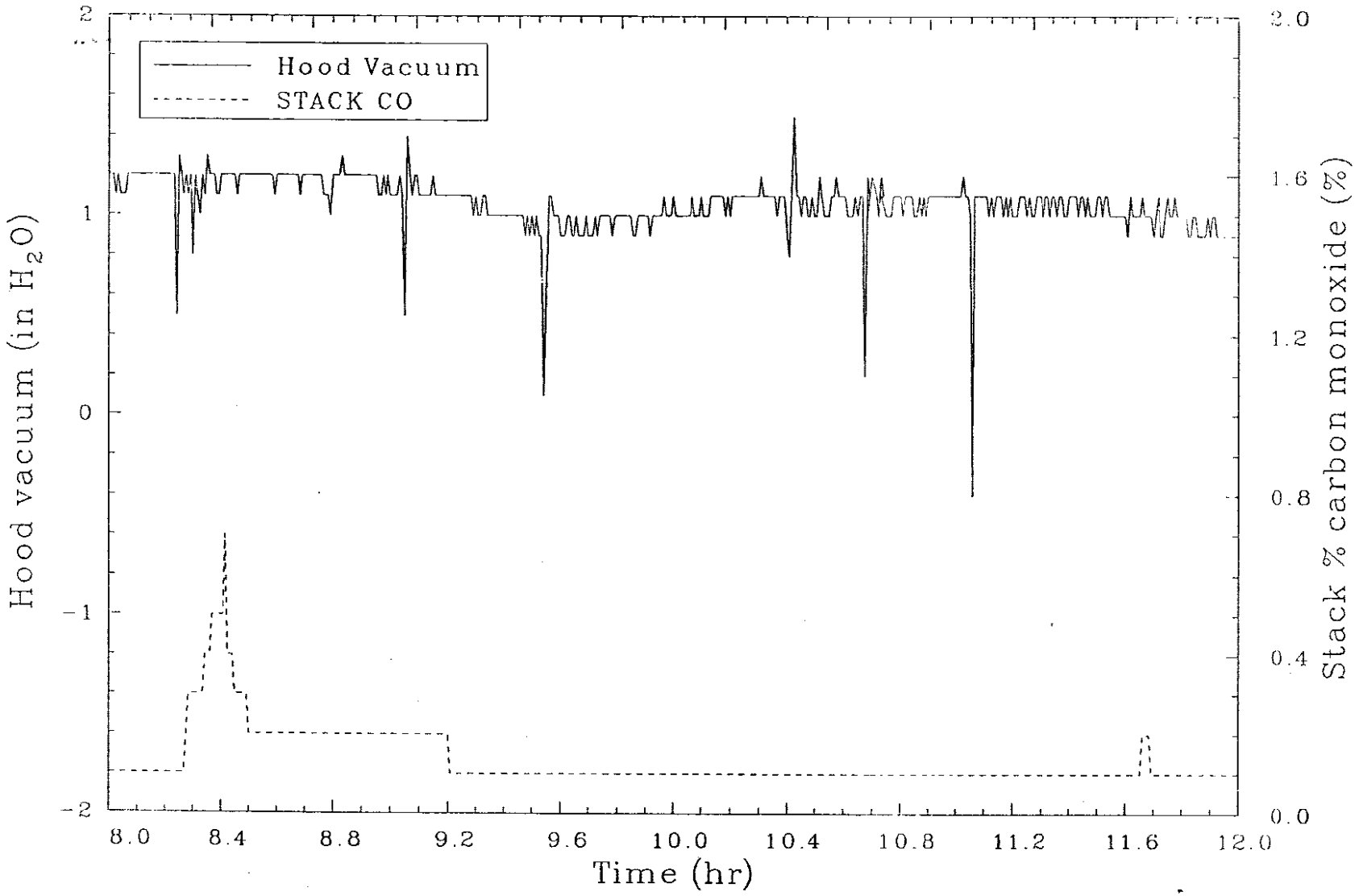

Figure 33. Hood vacuum and stack carbon monoxide concentration for Test 1, showing pressure events not concurrent with CO spikes.

- The off-gas temperatures in the hood fluctuated dramatically with each encounter of a container. As a result, the gas heater, designed to reheat the gas stream following wet scrubbing, required careful monitoring and frequent adjustment. Without this adjustment, excessively low gas temperatures would result in condensation in the HEPA filters, while excessively high temperatures would result in challenging the high maximum temperature limits for the blower. The present large-scale machine has an automatic set point controller that would effectively respond to these fluctuations.

- The rapidly fluctuating hood vacuum caused the automatic surge protection valve for the blower to continually readjust its position. The surge protection valve allows a controlled air flow into the blower to supplement the off-gas flow in cases of low gas flow from the hood. The effect of a low gas flow causes blower amperage to increase, potentially creating blower cavitation. When the surge protection valve was open, dilution of the off-gas flow resulted in a false high total off-gas flow value and a dilution of the off-gas stream prior to the stack measurements of CO, CO_2 and O_2.

3.3.5 Melt Behavior at Each Event

Understanding the behavior of the melt at each event is fundamental to understanding the processing impacts on the containment, off-gas treatment, and electrical system. This understanding is essential to proceed with full-scale operations on actual sites containing buried wastes. To fully detail the information gained from Test 1, qualitative visual observations are combined with measured data to provide a more explicit understanding of buried waste processing. Several of the events involving gas release from the containers are characterized below using the following key inputs.

- Hood temperature and pressure data

- Off-gas data including CO and O_2

- Amperage, voltage, and power to the electrodes
- Electrical resistance in the melt
- Visual observations during operations
- Posttest observations during excavation activities.

3.3.5.1 The Initial Event. The initial event occurred at approximately 5.9 hours into the test and resulted in the most dramatic temperature and pressure spikes for the test. In this event glass was ejected from the melt and contacted the hood surfaces at several locations including the tip of the plenum thermocouple. A hood vacuum plot of the event is provided as Figure 34. This event resulted in the most dramatic temperature spike (see Figure 23) even when accounting for glass contact on the plenum thermocouple. Figure 35 is a plot of roof and wall temperatures for several events and shows the dramatic temperature spike created by this initial event. The hood vacuum rapidly decreased during the event due to a rapid gas release from the melt, decreasing from an initial value of 0.9 in. of water to greater than 5.0 in. of water pressure. The pressure transducer range was from +5 to -5 in. of water; consequently, the exact magnitude of the pressure spike cannot be quantified. However, based on an estimate of the slopes when the data set is greatly expanded, the spike appears to have achieved a positive pressure of approximately 7 in. of water pressure.

At the time of the event, operators responded by deenergizing electrode power. Once power was reenergized, power levels had decreased approximately 100 kW, as shown in Figure 36. Resistance in the melt, as calculated from measurements in the secondary windings of the transformer, increased from 2 to 20 ohms on phase A and from 2 to 4 ohms on phase B, as shown in Figure 37. This difference in resistance on the secondary windings suggests the event had a localized effect adjacent to a phase A electrode. Resistance data both during startup and at later times in the test show the phases A and B resistance values agreed closely, as expected. Therefore, there is confidence in the resistance measurements indicating a localized effect on a phase A electrode. Resistance gradually returned to pre-event levels, approximately

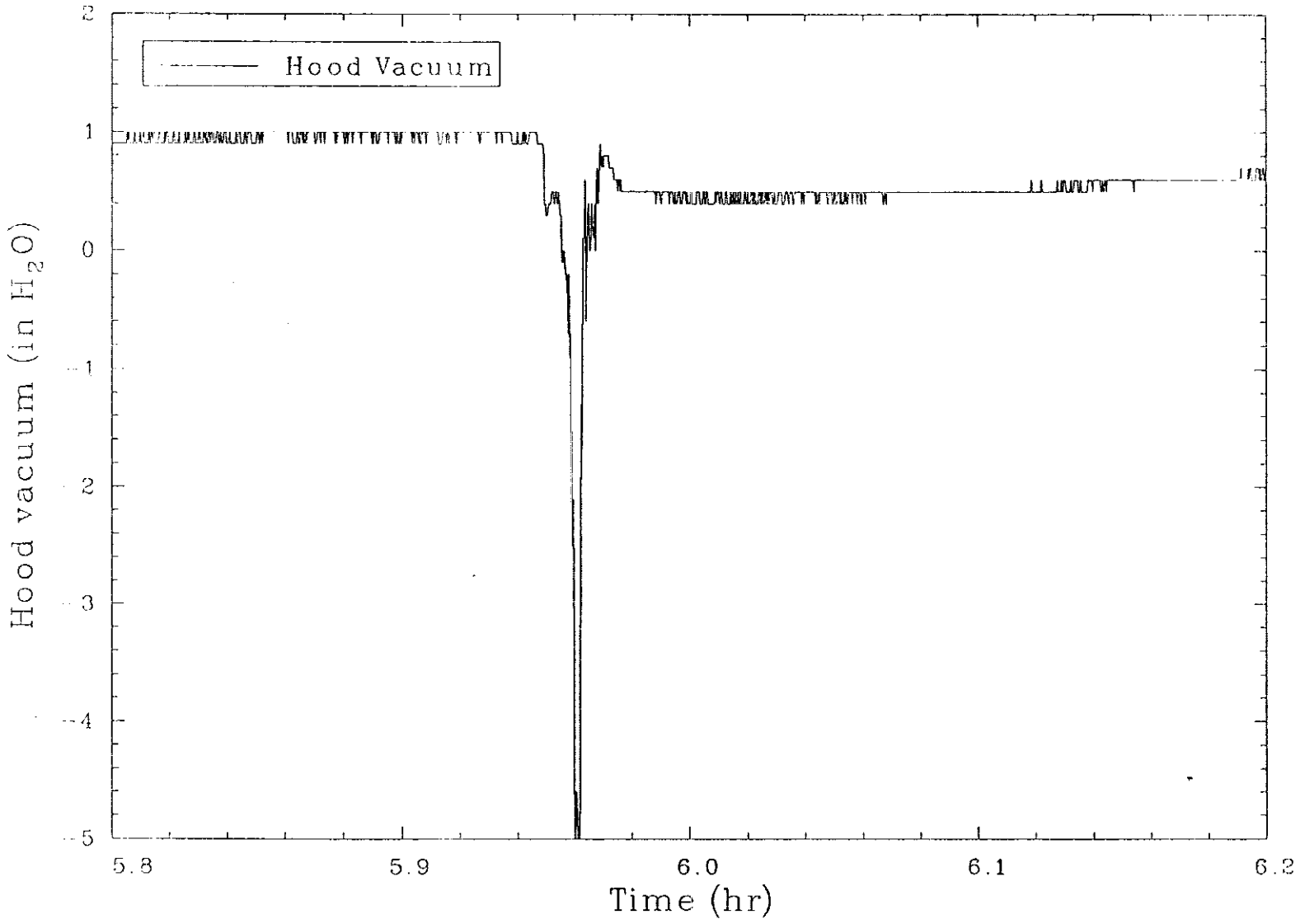

Figure 34. Hood vacuum for the initial gas release event in Test 1.

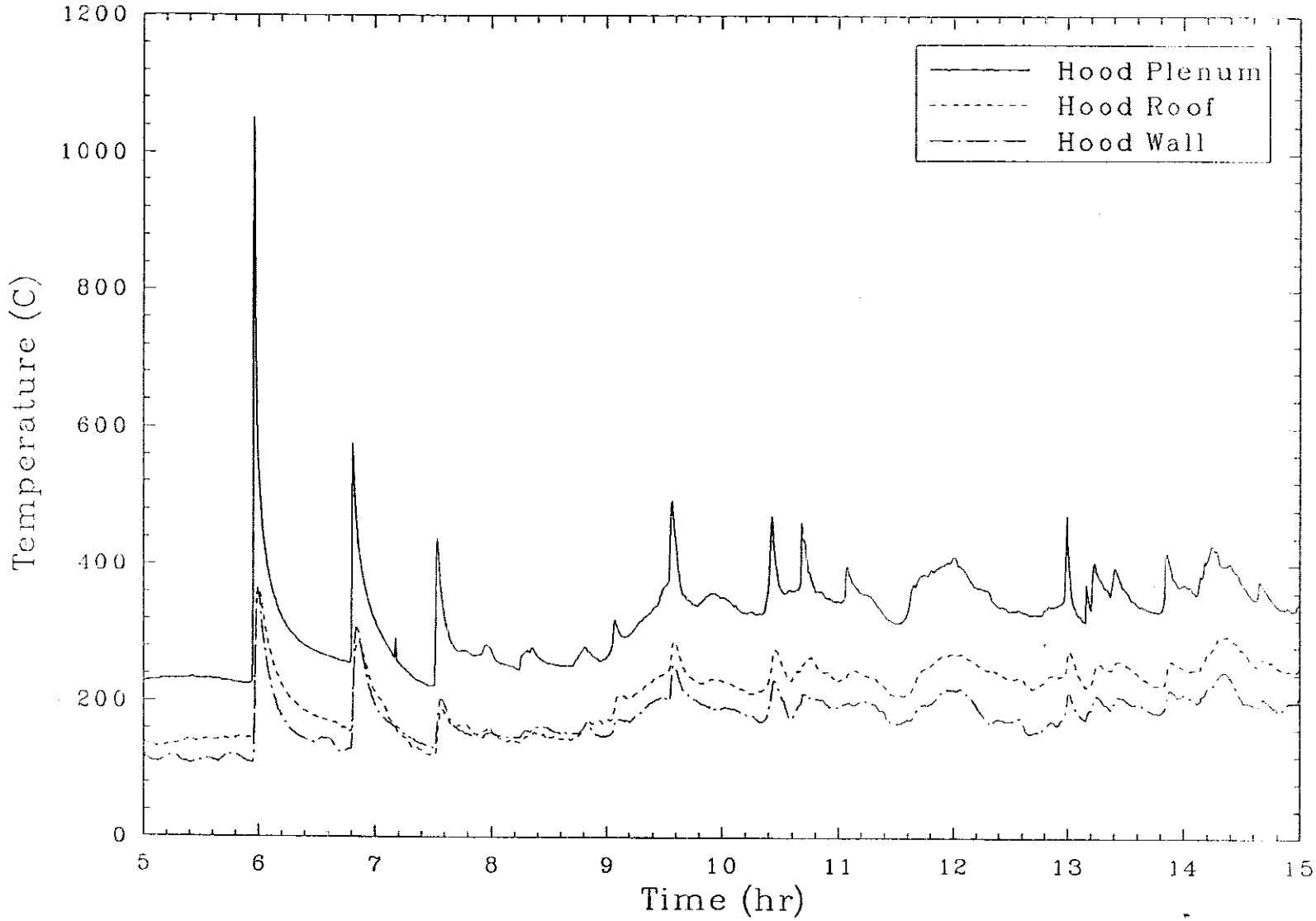

Figure 35. Hood, roof, and wall temperatures for several gas release events in Test 1.

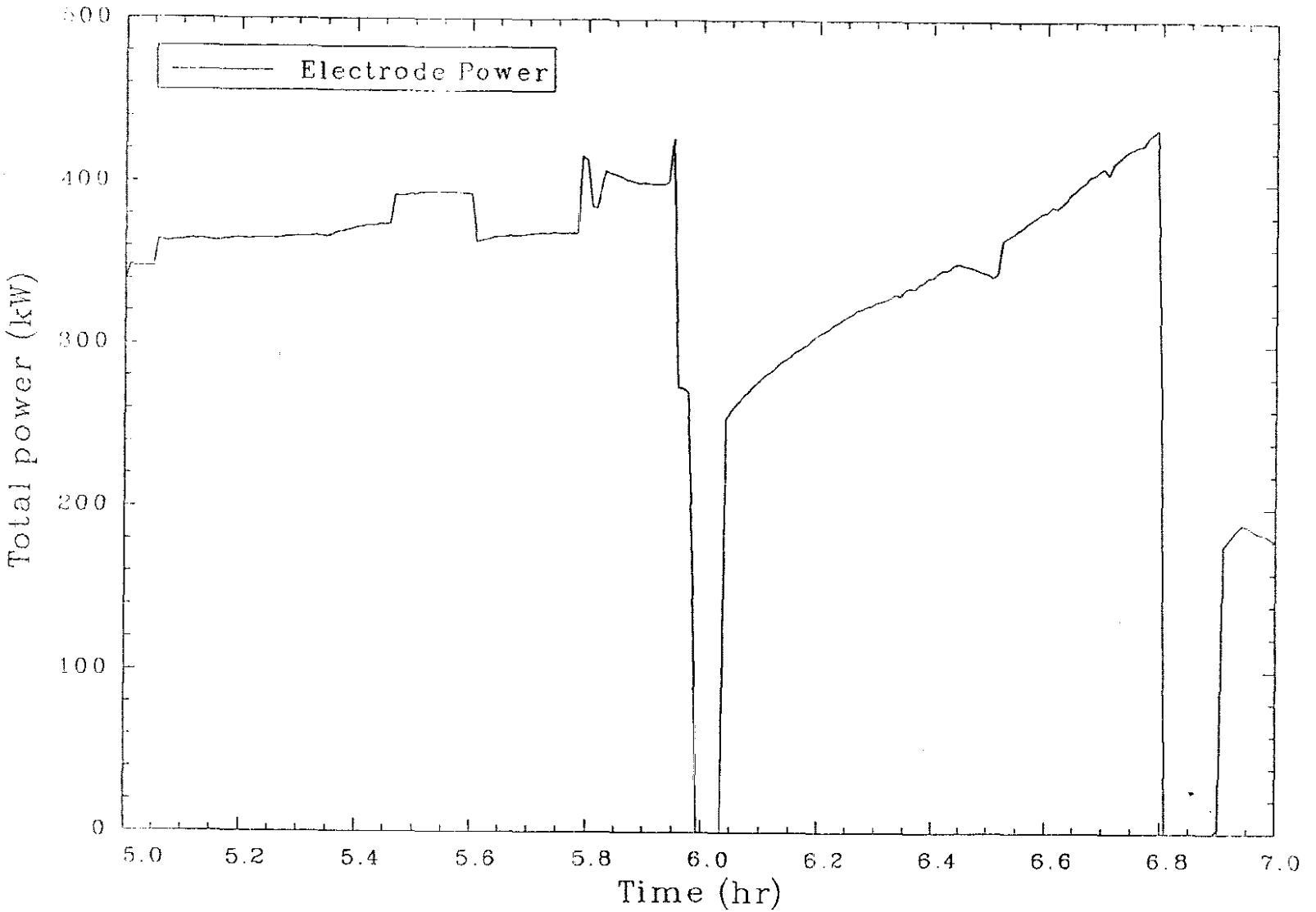

Figure 36. Total electrode power for Test 1, showing power level decrease after the initial event.

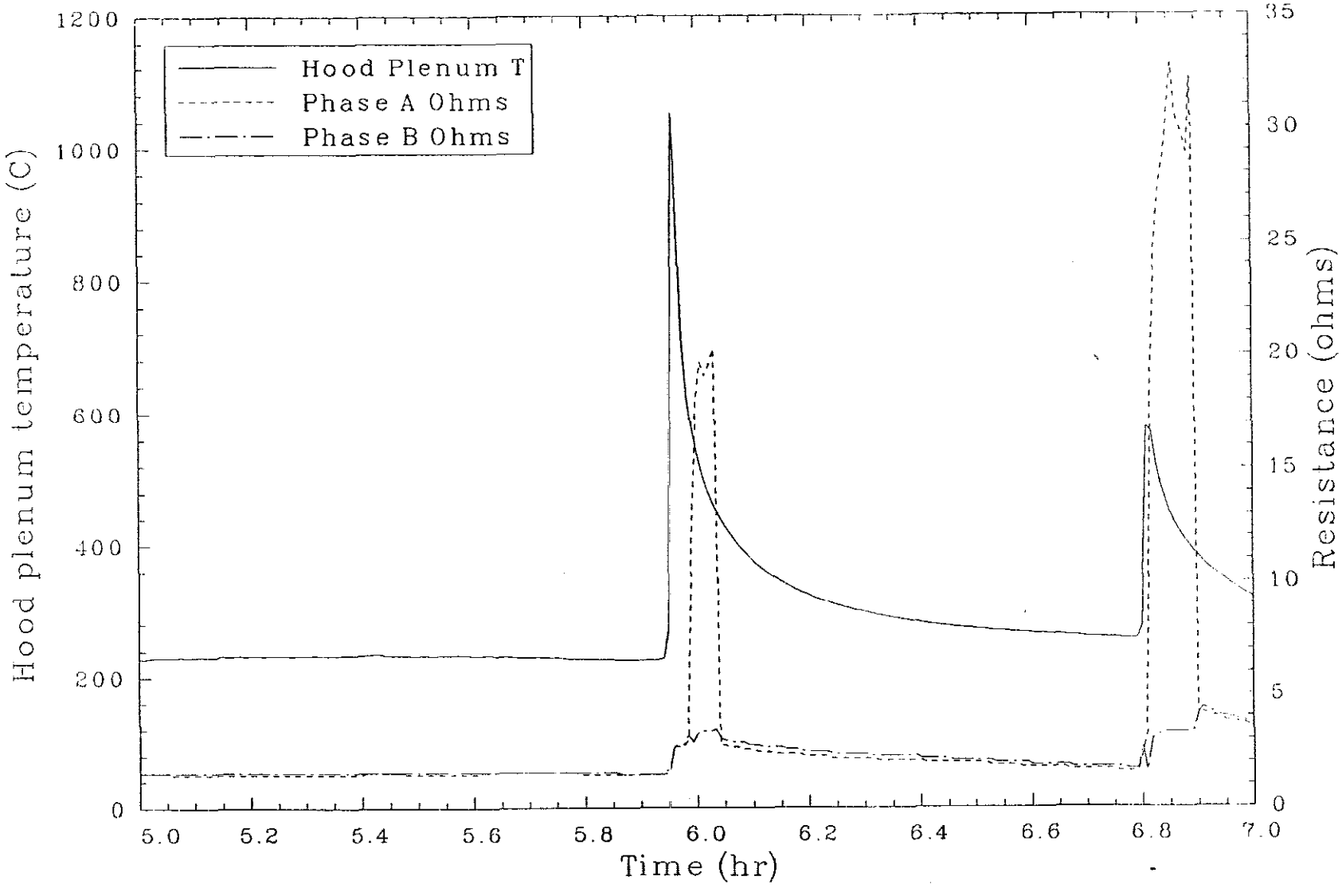

Figure 37. Phase A and B resistance during the initial gas release event in Test 1.

6 minutes after the event. Possible explanations for the single phase resistance increase include:

- The insulation blanket, placed during the laying of the starter path, subsided into the melt (as observed by the operating staff) and settled into a position that partially disrupted the firing pattern of a phase A electrode.

- A gas release caused a localized cooling effect on the glass. Any gas release through molten glass would act to remove heat from the glass and disrupt the cold cap, creating a situation where the molten glass could loose heat radiantly. Due to convective mixing currents in the melt, a localized area of cooled glass could be mixed, and increased resistance would be observed on both phases. As shown in Figure 37, resistance on phase B increased from 2 to 4 ohms.

- A portion of the frozen glass comprising the cold cap dislodged and caused partial disruption of the conductive path while serving to locally cool the glass. Once the frozen glass melted, the convective mixing currents in the melt would ultimately balance the resistance over both phases.

Other possible explanations that were discounted included the presence of electrically disruptive gas bubbles in the melt and the actual loss of glass volume due to ejection or glass flow into containers adjacent to the melt. These explanations are discounted because the bubbles would cause only a momentary electrical disruption before being released from the melt. In addition, glass flow away from the melt to an adjacent container would tend to affect both phases equally, as would the case where molten glass was ejected from the melt.

Carbon monoxide concentrations indicate that a significant volume of combustible gasses burned in the hood during the transient event. Carbon monoxide values at the stack spiked from 0 to 0.2% and then returned to 0%, as

shown in Figure 38. Oxygen concentrations dropped to just under 12%, which was the lowest level observed during the test.

Operating staff observed the following during and immediately after the event.

- A few localized points of glass contacting the interior surfaces of the hood were observed as glowing red spots from the exterior of the hood.

- The event caused the upper portions of the 304L stainless steel sheet metal panels on the hood to discolor to a bronze or copper color during the event.

- Visual observations through the viewing window in the hood immediately after the event revealed the insulation blanket had been covered by molten glass, causing the blanket to sink into the melt out of sight. Molten glass was ejected from the melt with sufficient force to contact most surfaces of the hood including the roof, plenum thermocouple, side panels, and the door.

This first event provided valuable information on the relationships of hood temperature and pressure relative to containment, resistance and power response data relative to a Scott-Tee transformer, and gas concentrations relative to the off-gas treatment system design. It is evident that the off-gas hood for a large-scale machine must be designed to handle dramatic temperature and pressure spikes and withstand direct contact with molten glass. Based on current large-scale transformer designs that include independent control on each phase of the secondary, imbalances on the secondary side of the transformer could be easily handled.

3.3.5.2 The Second Event. A second event occurred at approximately 6.8 hours into the test. This event resulted in the a dramatic hood pressurization similar to the initial event. Hood pressure spiked from 0.9 in. of water vacuum to over 5.0 in. of water pressure, as shown in Figure 39. The pressurization was followed by a temperature spike from 260 to 600°C.

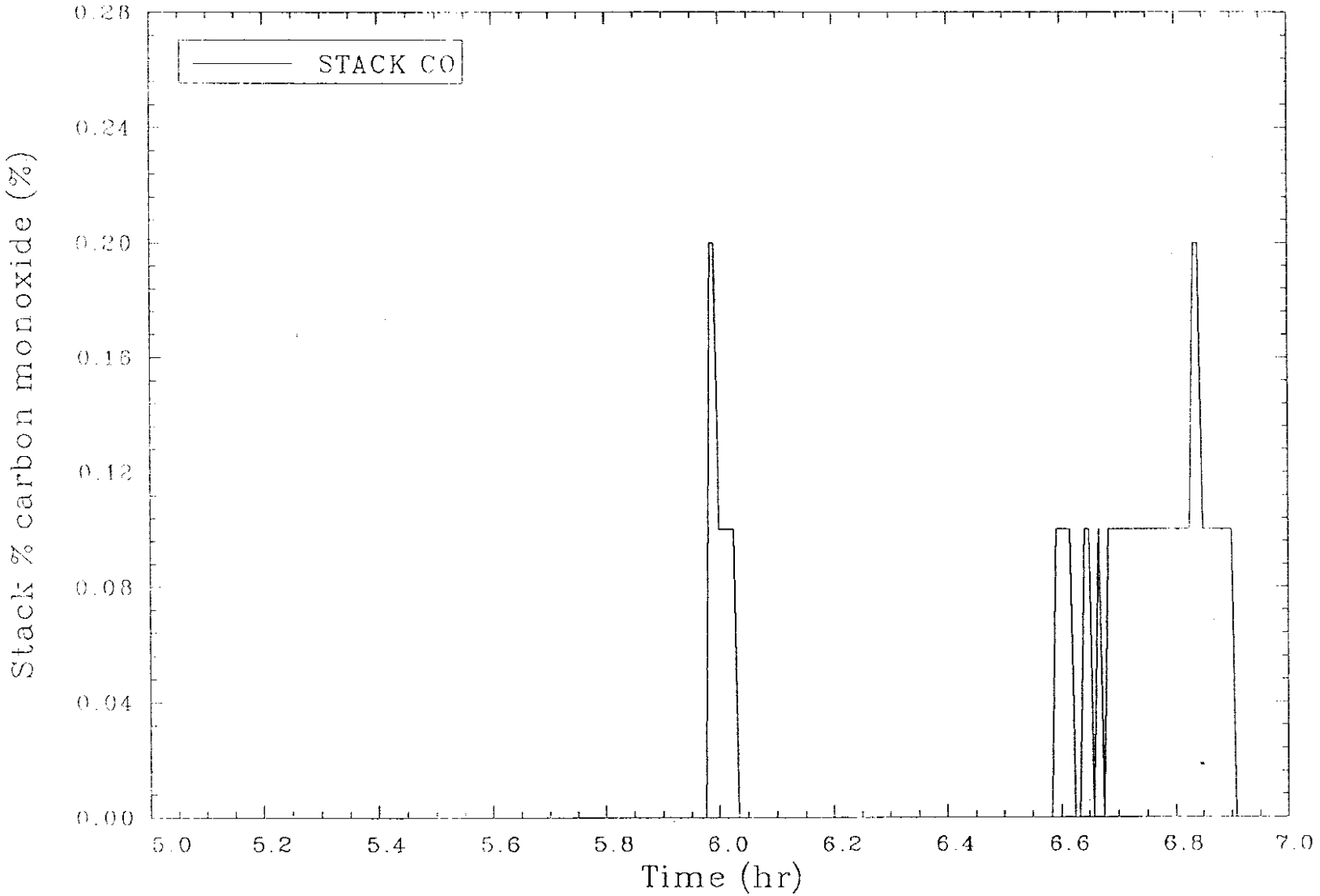

Figure 38. Stack carbon monoxide concentration during the initial gas release event in Test 1.

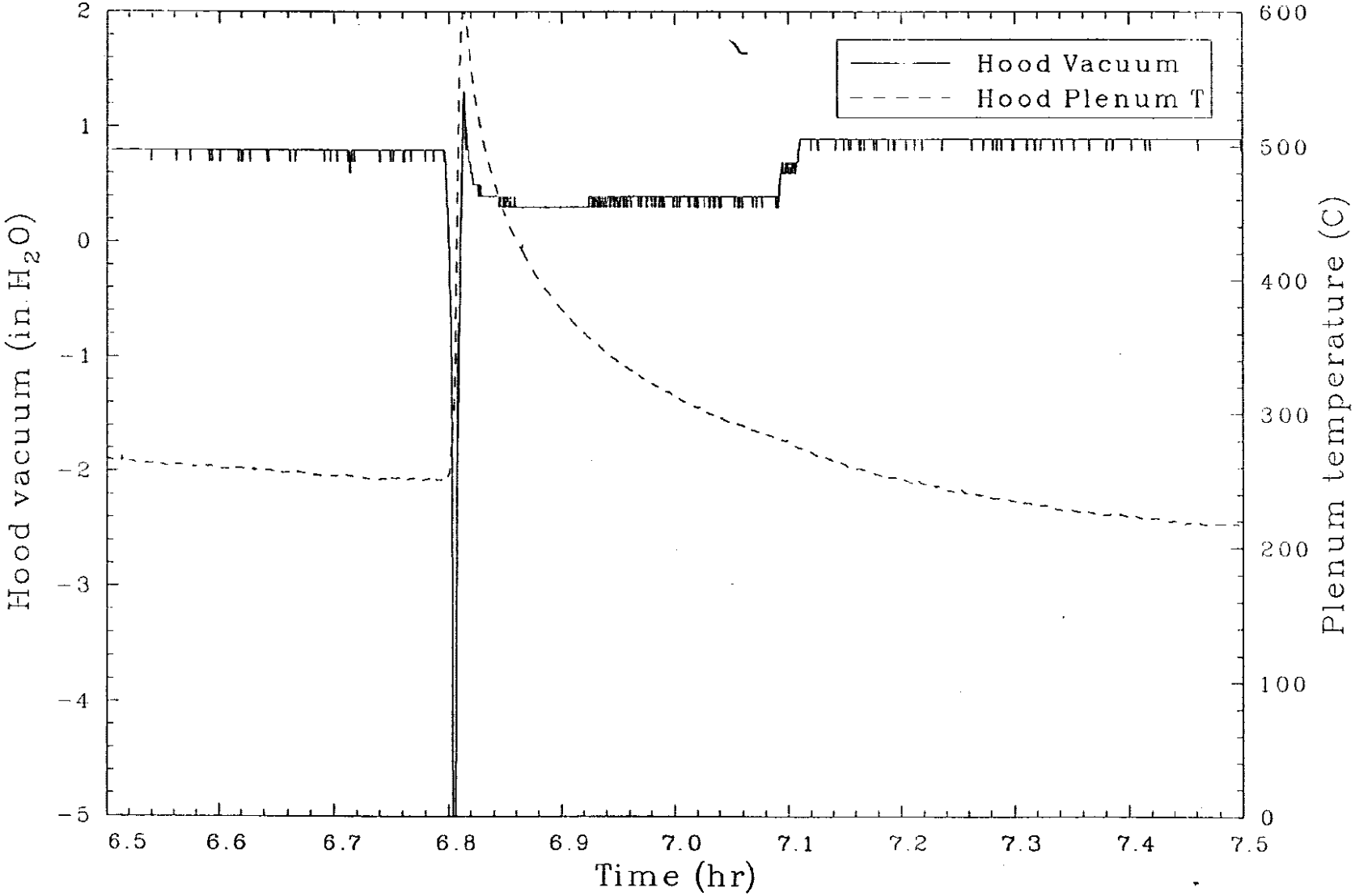

Figure 39. Hood vacuum and plenum temperature during the second event in Test 1.

Operators observed smoke escaping from the hood around the base of the hood and out through the HEPA filtered seal pot. Soil providing a seal at the base of the hood by the door was dislodged as pressure was relieved from the hood. Carbon monoxide concentrations at the stack increased from 0.1 to 0.2%, and oxygen concentration dropped from approximately 20.5 down to 17.5%, indicating that significant combustion occurred in the hood, shown in Figure 40.

Electrical resistance data from this event are similar to the initial event. Phase A ohms increased from 2 to approximately 33 ohms while phase B increased from 2 to 5 ohms, as shown in Figure 41. Phase A amperage decreased from approximately 400 to 160 A, as shown in Figure 42. Figure 43 illustrates the total power of the test decreasing from 440 to 180 kW as a result of the event. Even when accounting for a nonpowered period of operation immediately following the pressurization, phase A resistance dramatically increased, while phase B resistance increased only moderately. This again suggests a localized effect on one of the two phase A electrodes.

Like the first event, this second event provided valuable information on the relationships of hood temperature and pressure relative to containment. In addition, the magnitude of the pressurization identifies the need for a fast acting, high capacity pressure relief device that can effectively treat gases prior to their release from the hood.

3.3.5.3 The Third Event. The third event occurred at approximately 7.5 hours and resulted in only moderate plenum temperature and hood vacuum spikes relative to the first two events. The plenum temperature increased from approximately 220 to just over 440°C. The hood vacuum spiked from 1.2 to 0.6 in. of water. Figure 44 shows the temperature and vacuum relationship for this third event.

Electrical resistance data was balanced, unlike the previous two events. Phases A and B increased from 2 ohms to just over 4 ohms as a result of the event, shown in Figure 45. Power was not interrupted by operators during the event. Phase A amperage dropped from 320 to 160 A; and phase B amperage dropped from 300 to 140 A, as shown in Figure 46. Total power dropped from

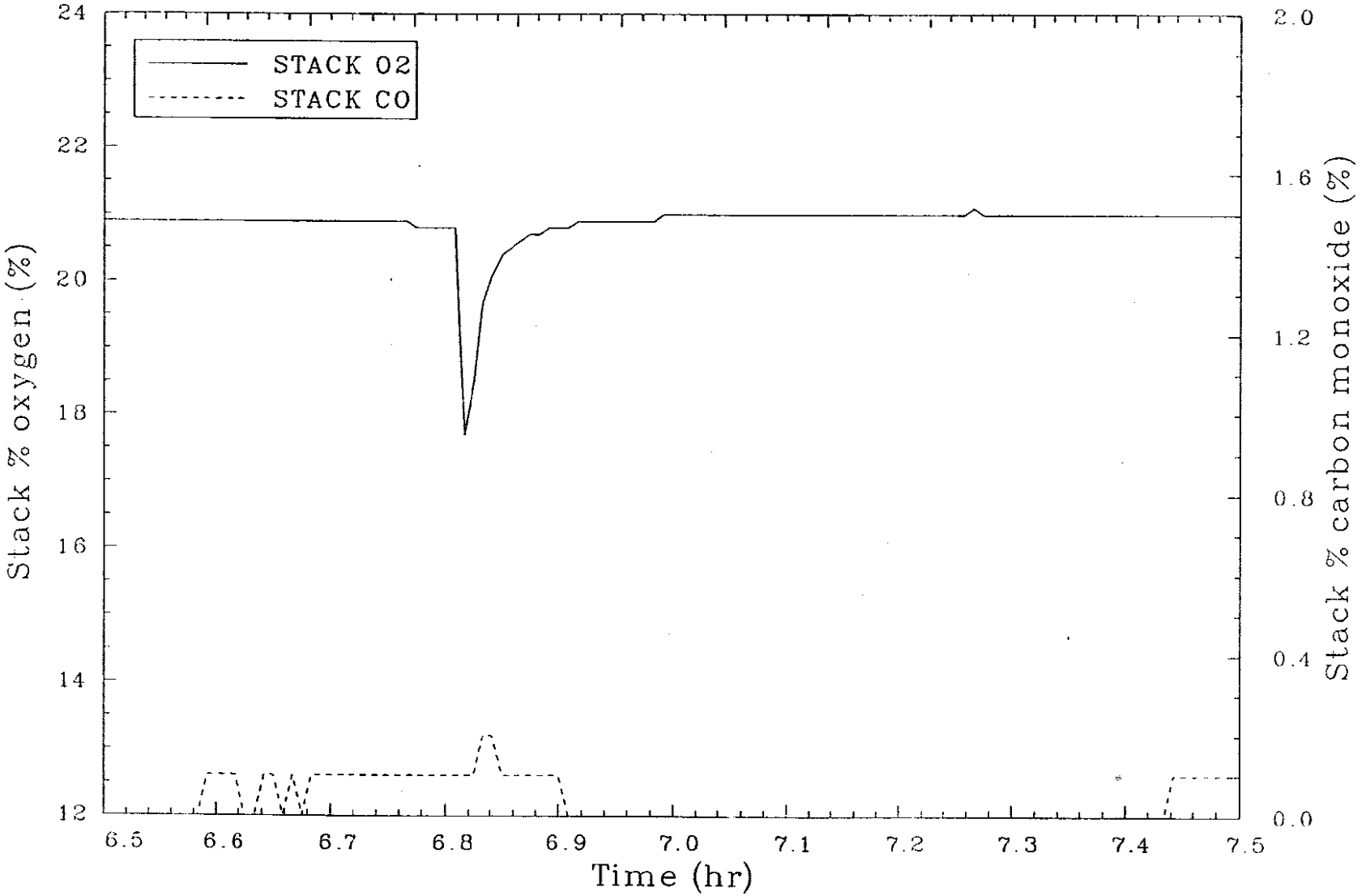

Figure 40. Stack oxygen and carbon monoxide concentrations during the second event in Test 1.

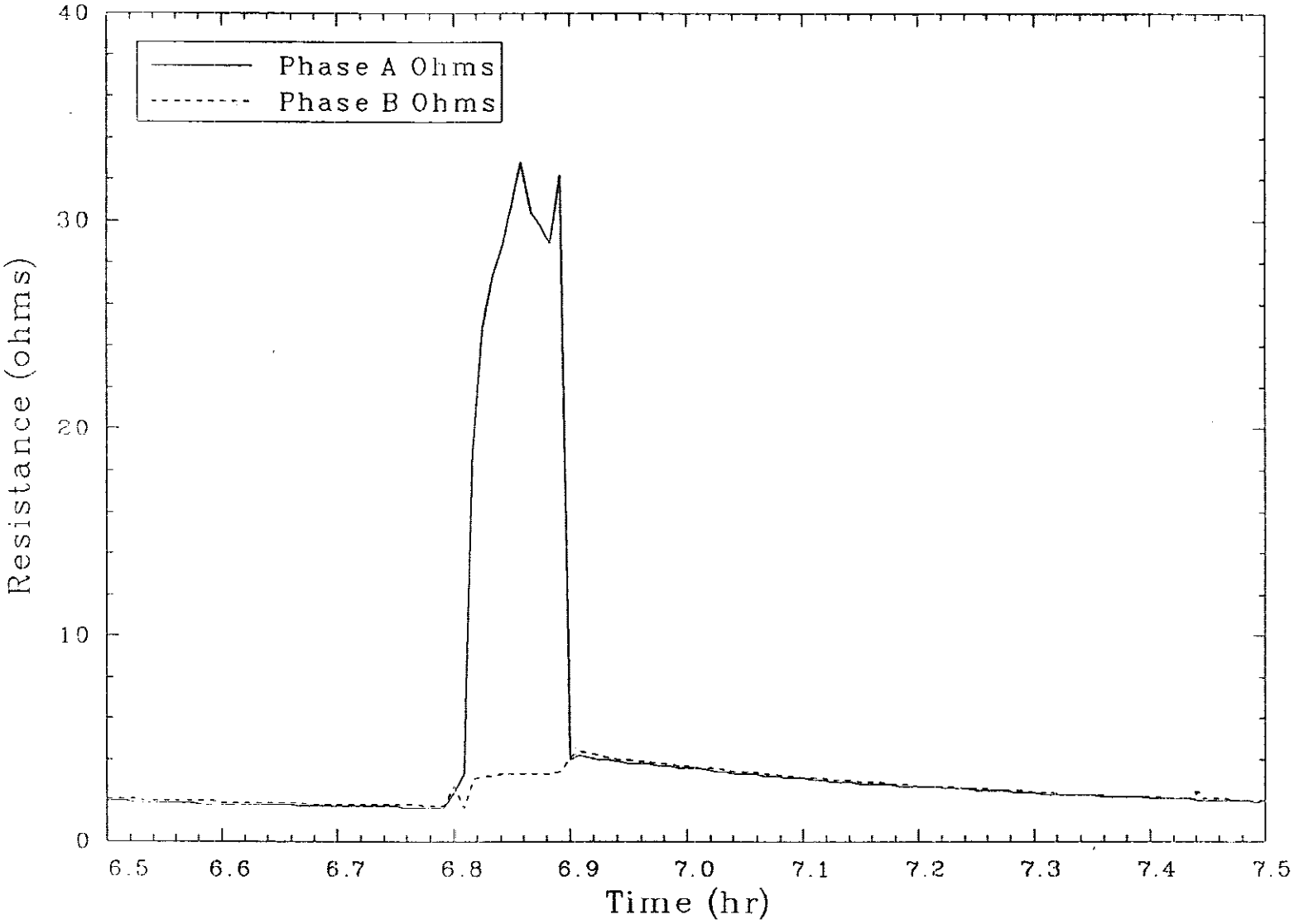

Figure 41. Phases A and B resistance during the second event in Test 1.

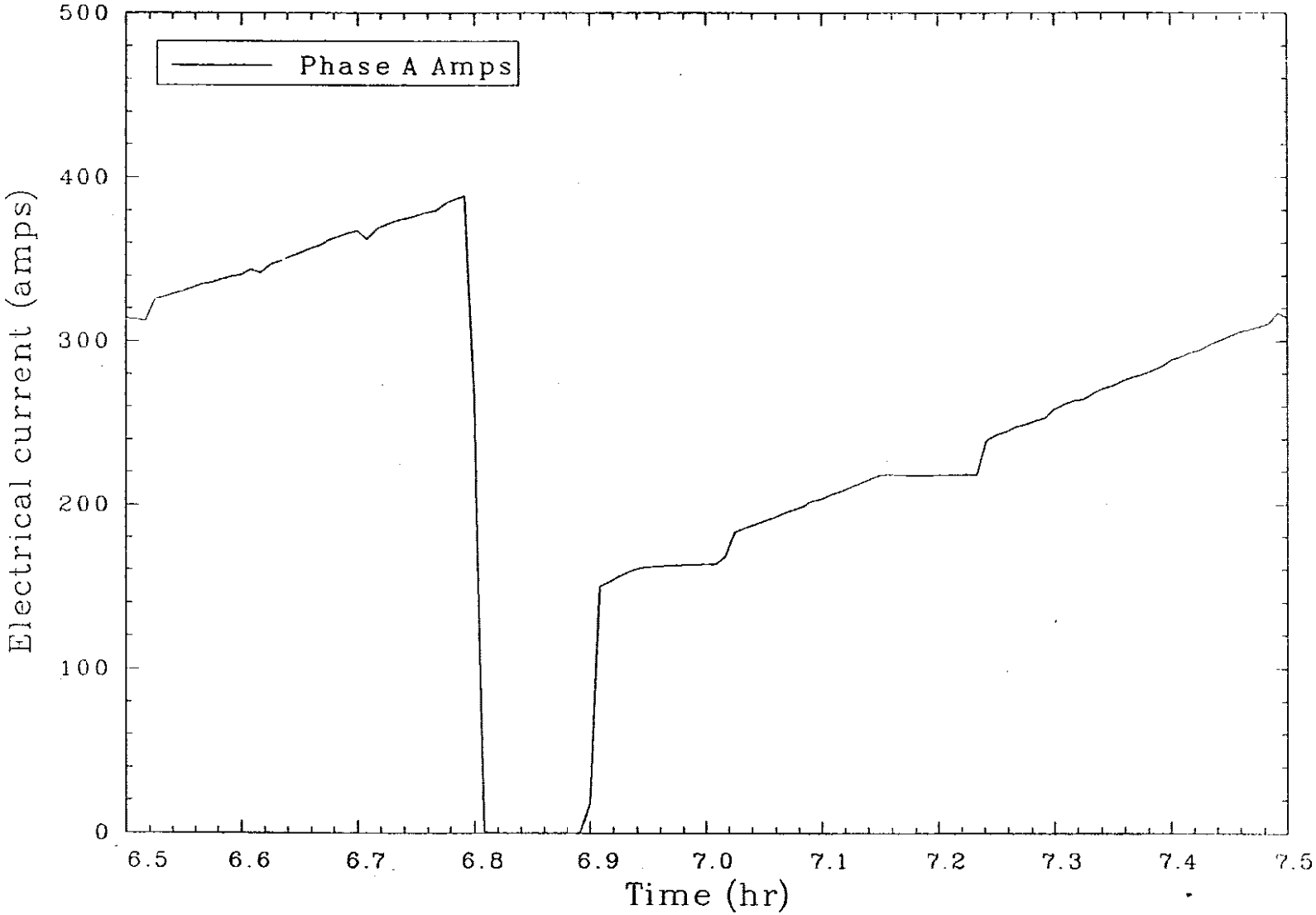

Figure 42. Phase A amperage during the second event in Test 1.

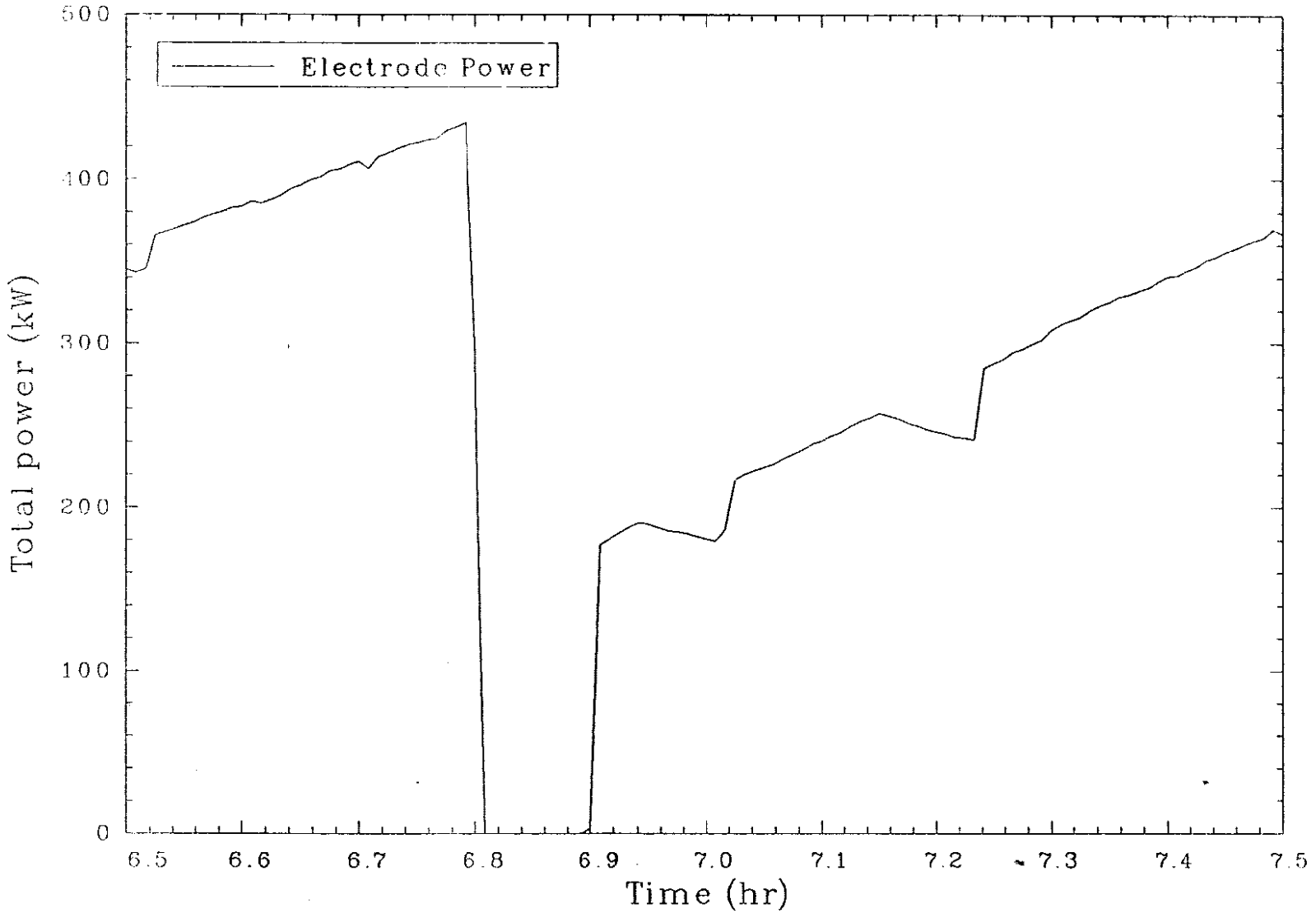

Figure 43. Total electrode power during the second event in Test 1.

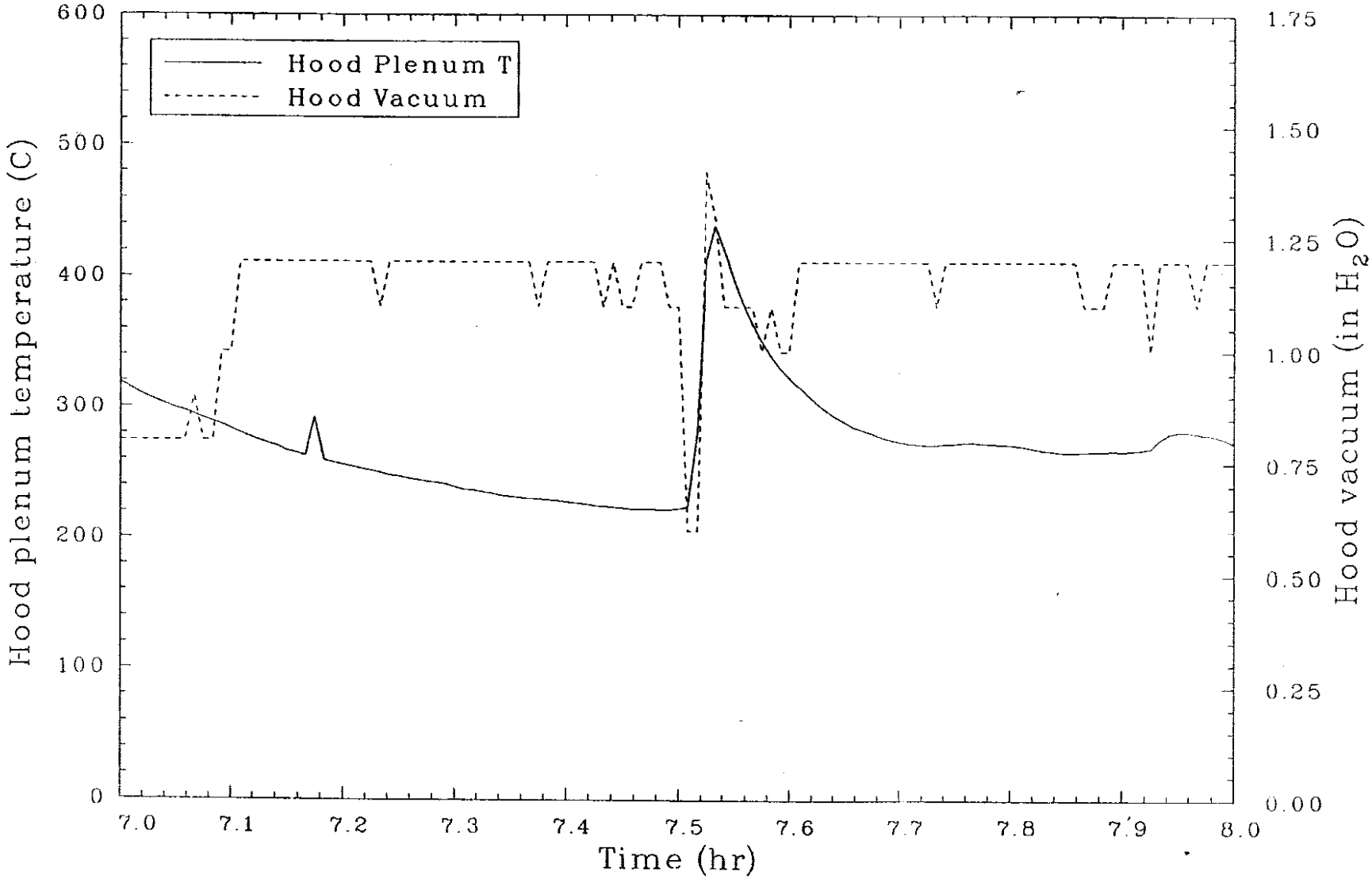

Figure 44. Hood vacuum and plenum temperature for the third event in Test 1.

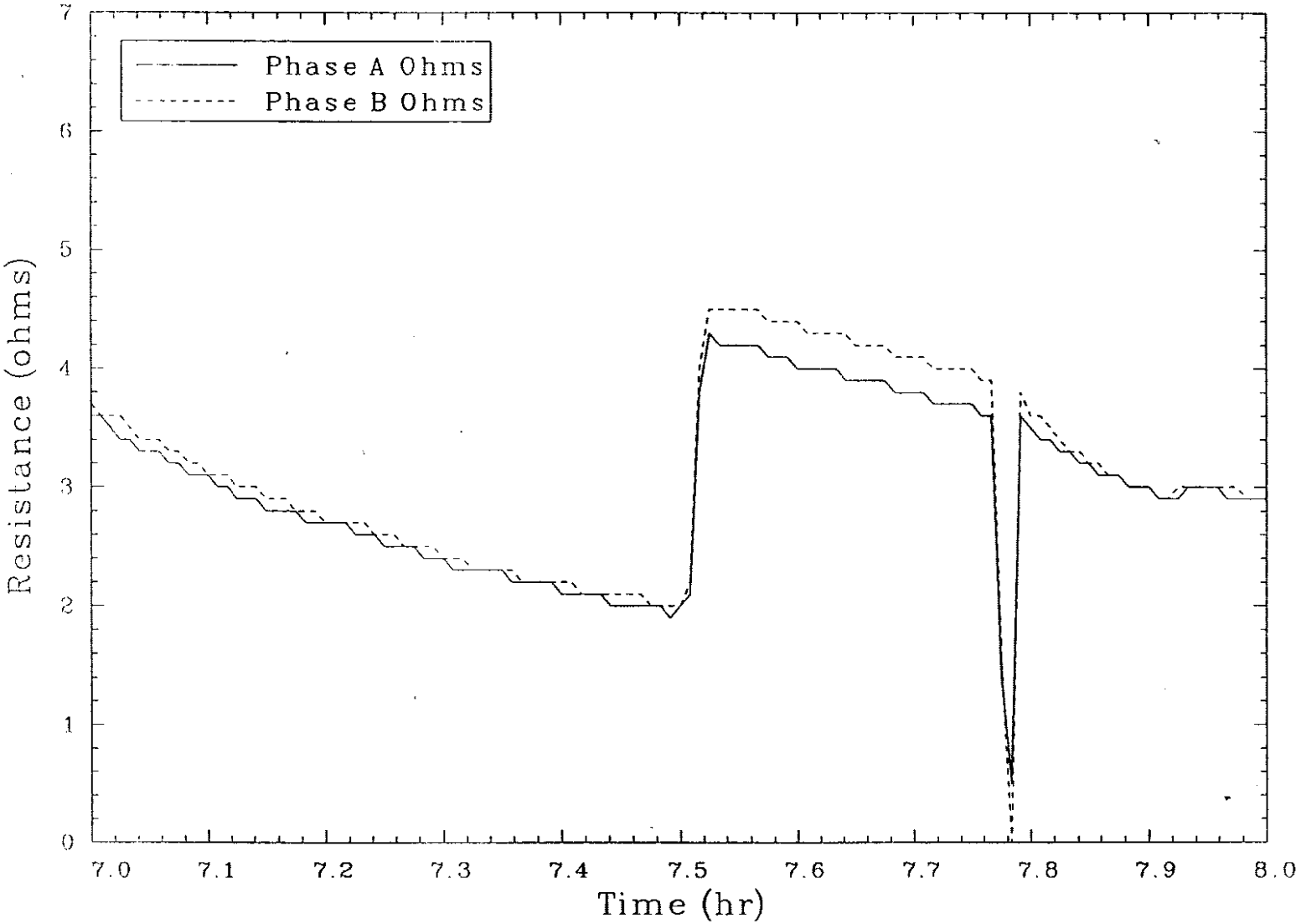

Figure 45. Phases A and B resistance for the third even in Test 1.

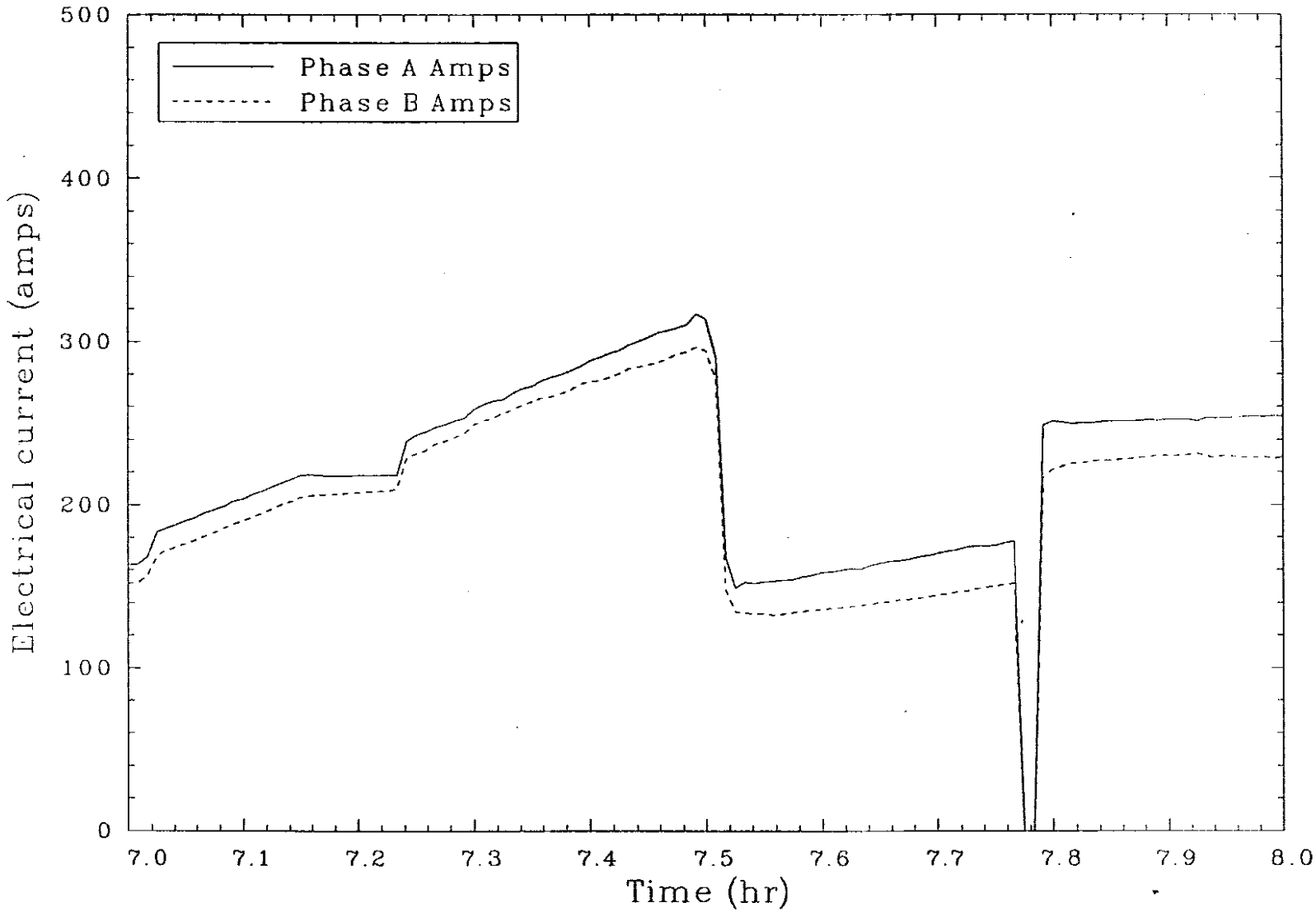

Figure 46. Phase A and B amperage for the third event in Test 1.

370 to 180 kW as a result of the event; this loss of power is illustrated in Figure 47. Radiant heat losses from the molten glass resulted in increased resistance in the molten glass as the glass cooled. This phenomenon occurred during essentially all gas releases (see Figure 23, p. 58).

Operators noticed resistance values rising sharply and immediately went to the hood to observe the event. A large opening, approximately 0.6 m (24 in.) in diameter, had formed in the center of the cold cap. Extremely hot molten glass was flowing up from the opening and covering the frozen cold cap. Within a few moments, the cold cap was completely covered by molten glass and disappeared from sight. Dissolution of the cold cap would explain the balanced increase in resistance on both phases because the overall melt temperature decreased with the introduction of pieces from the frozen glass layer into the melt.

The third event resulted in the stack oxygen concentrations to decrease from 20.9 to 16%, and carbon monoxide values to increase from 0 to 0.3%, shown in Figure 48. These values indicate the gas release resulted in combustion in the hood. An operator observed the event and noticed the hood appeared to be smoke filled. Flares were present.

3.3.5.4 Later Events. Several of the events later in the test involved hood vacuum fluctuations without any recorded change in the stack carbon monoxide concentrations. It is suspected the gas releases into the hood came from cans containing wet sludge. Once these cans were heated and pressurized, their resultant release to the hood consisted primarily of steam, hence, the steady state of carbon monoxide concentration. The oxygen concentration decreased from 20.3% to between 18 and 19% due to steam displacing the oxygen in the hood or to steam limiting the inflow of air to the hood during steam release from the melt (see Figure 31). Three events at approximately 9.5, 10.5, and 11.5 hours illustrate this phenomenon. Figure 33 is a plot of carbon monoxide concentration at the stack versus hood vacuum. The baseline carbon monoxide concentration of 0.1%, from 8 hours through 32 hours (see Figure 32), probably results from a gradual decomposition and combustion of organic materials from various cans and boxes; in particular, wood pyrolyzes more

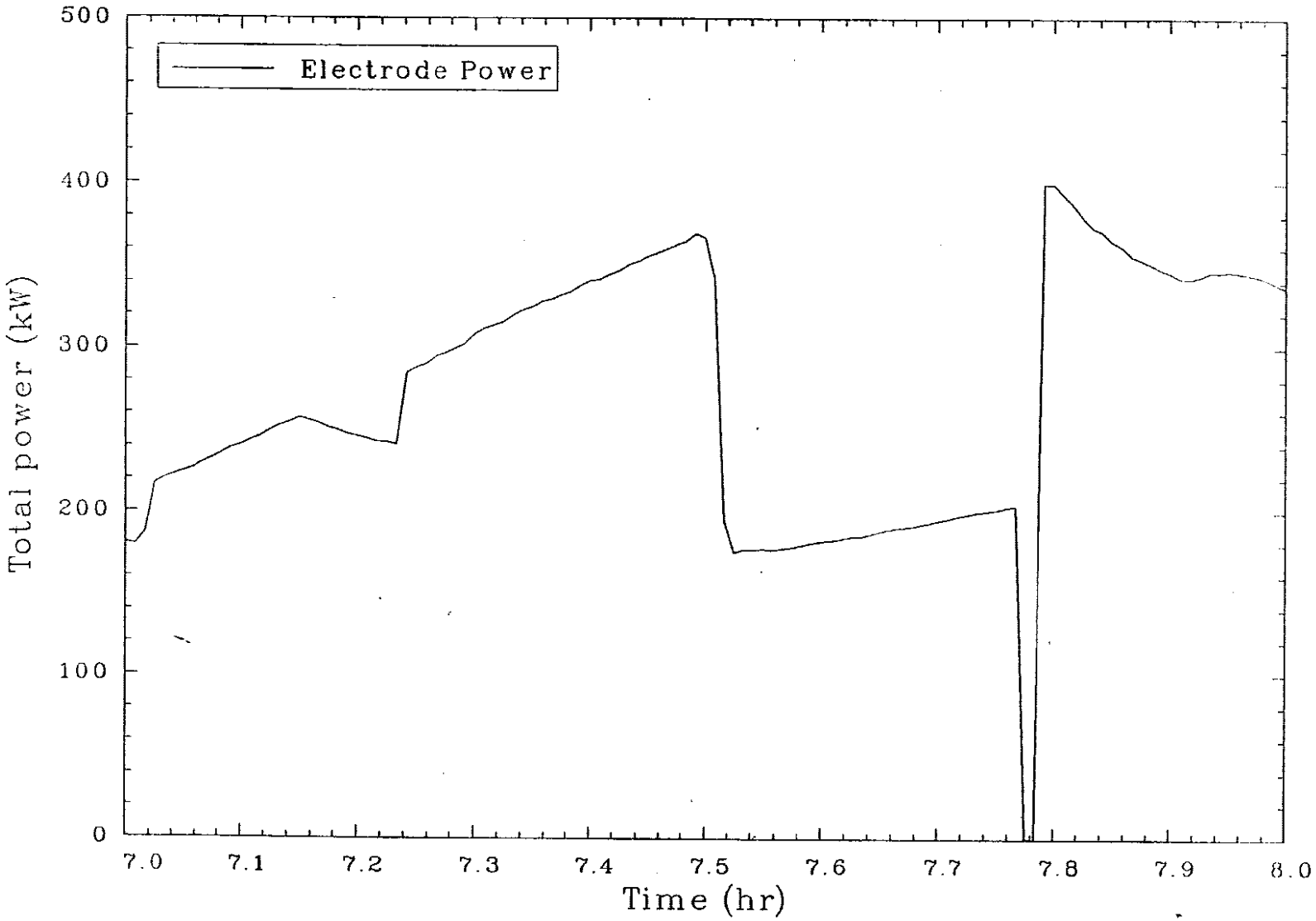

Figure 47. Total electrode power for the third event in Test 1.

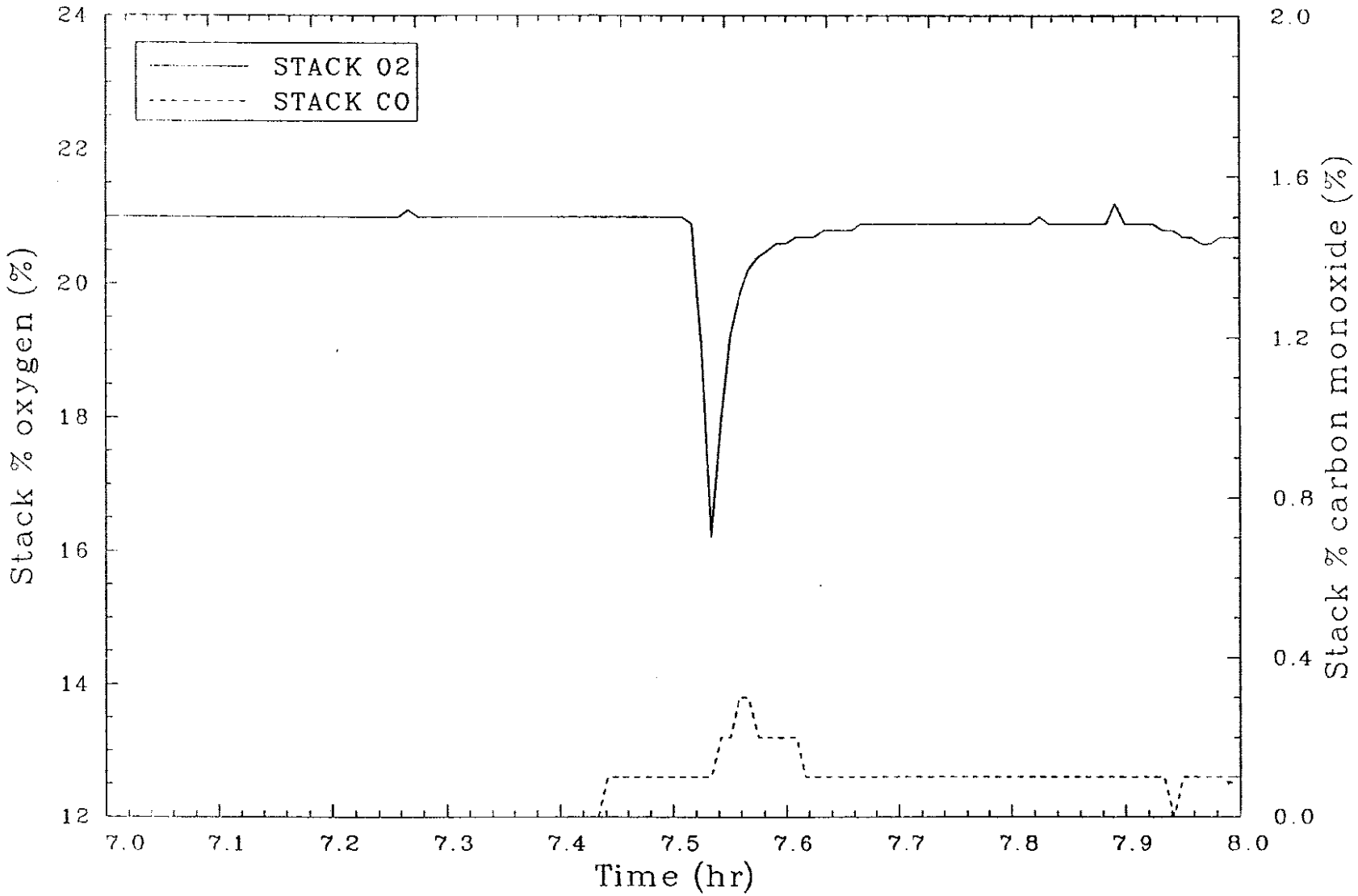

Figure 48. Stack oxygen and carbon monoxide concentrations for the third event in Test 1.

slowly than loosely packed paper or cloth. At approximately 11.3 hours, two operators observed what appeared to be a piece of charred wood floating on the melt.

3.3.6 Electrical Instabilities

As indicated in Section 3.3.2, one of the key problems associated with the test involved the use of the electrode coating used to limit oxidation of the graphite. This coating caused the electrodes to stick to the cold cap and ultimately contributed to the termination of the test shortly after achieving an approximate 2.4 m (8 ft) depth. The process suffered from electrical imbalances due to the inability to adjust the electrode positions. The imbalances created excessive heat in the transformer and caused saturable core reactor fuse and thyristor switch failures. The total power supplied to the melt at 22 hours into the test was 54 kW on phase A and 5 kW on phase B. It was evident that a phase B electrode was not sufficiently contacting the conductive portion of the melt because phase B amperes were only 15% of the phase A amperes. As shown in Figure 49, at 23 hours into the test, phase A resistance equaled 8 ohms while phase B resistance equaled approximately 40 ohms. Over the next 6 hours, phase B resistance gradually increased to over 100 ohms while phase A resistance remained relatively constant at less than 6 ohms. Phase A resistance had decreased from 8 to 6 ohms due to heat being introduced by the phase A electrodes following the extended period of nonpowered operation to replace failed fuses and thyristor switches.

Attempts to replenish the heat to the melt via electrode power through phase A was futile and resulted in localized heating between the phase A electrodes. Phase A resistance gradually increased to 170 ohms, and the glass pool being heated by the phase A electrodes ultimately melted away from the four stuck electrodes. The test was terminated when phase A amperage began to wildly fluctuate while the phase A voltage correspondingly spiked to full-scale. This indicated the advancing melt had finally melted away from at least one of the phase A electrodes. At this point, because the electrodes were frozen in place and no longer in contact with molten glass, electrode power was terminated and preparations for process equipment shutdown were initiated.

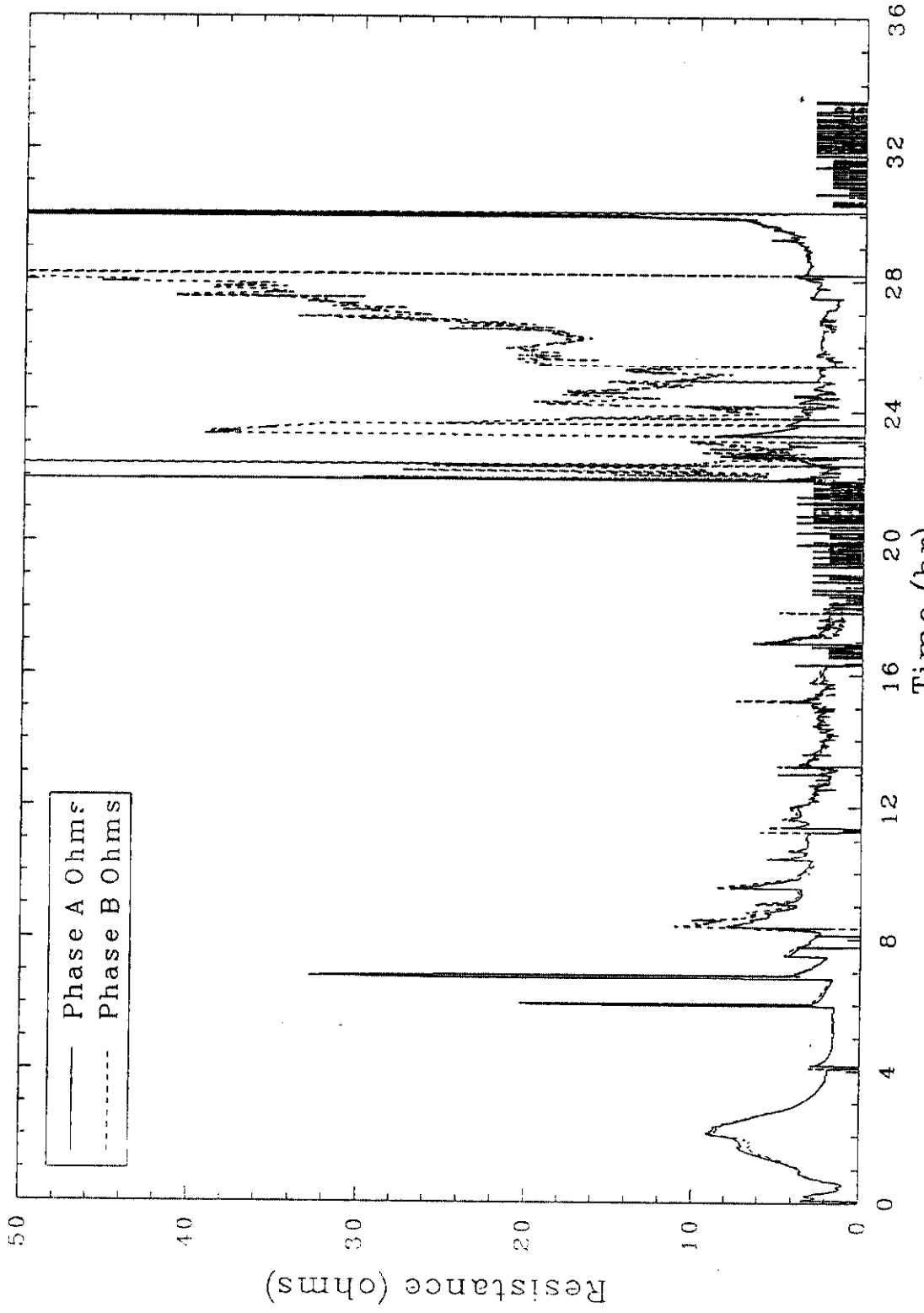

Figure 49. Phases A and B resistance for Test 1.